Received: 19 February 2021 | Revised: 15 June 2021 | Accepted: 18 June 2021

DOI: 10.1111/joa.13503

Journal of Anatomy ANATOMICAL SOCIETY WILEY

ORIGINAL PAPER

Intraskeletal bone growth patterns in the North Island Brown Kiwi (*Apteryx mantelli*): Growth mark discrepancy and implications for extinct taxa

Christian T. Heck | **Holly N. Woodward**

Department of Biomedical Sciences, Oklahoma State University – Center for Health Sciences, Tulsa, OK, USA

Correspondence
Christian T. Heck, Department of Biomedical Sciences, Oklahoma State University – Center for Health Sciences, Tulsa, OK, USA.
Email: ctheck@okstate.edu

Abstract

Osteohistology, the study of bone microstructure, provides an important avenue for assessing extinct and extant vertebrate growth and life history. Cortical vascularity and collagen fibre organization are direct reflections of growth rate, while bone growth marks are indicative of absolute age. However, each skeletal element has its own ontogenetic trajectory and microstructure of certain bones may not be a true representation of whole body growth. Extensive comparative study of modern taxa is required to resolve intraskeletal discrepancies among age, vascularity and tissue organization in extinct vertebrates. Despite their comparative utility, studies of bone microstructure in modern taxa are severely lacking. Here, we add to a growing comparative osteohistological database by describing (1) bone tissue organization, (2) growth mark count, (3) sexually dimorphic bone (e.g. medullary bone) and (4) secondary cortical reconstruction in the bone microstructure of a 14-year-old male and 5-year-old female North Island Brown Kiwi (*Apteryx mantelli*). Transverse and longitudinal histological ground sections were processed and described for femora, tibiotarsi, tarsometatarsi, humeri, ulnae and radii in both kiwis. Cortical bone can generally be described as parallel-fibered tissue, interrupted by cyclical growth marks, with vascular canals oriented longitudinally within primary and secondary osteons. Tissue morphologically resembling medullary bone is present in the hindlimbs of the female, and coarse compacted cancellous bone (CCCB) is found sporadically in the male and female hindlimbs. Lines of arrested growth (LAGs) are present in all hindlimb bones of both kiwi, but remodelling has obliterated all LAGs in the male ulnae and radii. LAG count varies intraskeletally, but large weight bearing elements such as femora and tibiotarsi have less remodelling and, thus, higher number of LAGs. LAG count did not match absolute age in any skeletal element; a maximum of seven LAGs are present in the male kiwi and a maximum of seven LAGs in the female kiwi. The tissue organization within the forelimbs and hindlimbs is reflective of the protracted growth strategy of the North Island Brown Kiwi and congruent with previous studies of the kiwi. LAGs were highly variable throughout the skeleton of the kiwi and a decoupling of age and LAG deposition is apparent from the male kiwi samples. Excess LAGs in the 5-year-old female kiwi may be a product of hatching, egg laying or captivity. Regardless, LAG count variation in the kiwi stresses the importance of intraskeletal sampling when

assessing growth patterns of extinct taxa. An extensive ontogenetic sampling of kiwi is necessary for future investigations of bone growth patterns, CCCB formation, medullary bone and LAG deposition and obliteration in these elusive birds.

KEYWORDS
Apteryx, Aves, bone, growth marks, growth patterns, osteohistology, Palaeognath, skeletochronology

1 | INTRODUCTION

With the importance of applying osteohistology to investigations of extinct vertebrate growth dynamics now firmly established (see Bailleul et al., 2019; Kolb et al., 2015 for review), further refinements to understanding the relationships between bone biology and life history of present-day vertebrates become increasingly important for permitting more targeted inter- and intrataxic life history questions using the hard tissue fossil record (Bailleul et al., 2019; Houssaye, 2014; Kolb et al., 2015; Padian & Lamm, 2013 and references therein). For example, lines of arrested growth (LAGs) form annually within bone cortices of modern vertebrates (e.g. Castanet et al., 2004; Köhler et al., 2012) and, thus, are used to quantify age in extinct vertebrates (e.g. Lee & O'Connor, 2013; Turvey et al., 2005; Woodward et al., 2015). Ageing extinct vertebrates enable the study of population dynamics, physiology and ontogeny (e.g. Erickson et al., 2001; Lee & Werning, 2008; Woodward et al., 2015, 2020). However, intraskeletal variation in growth mark counts of modern taxa is rarely examined (e.g. García-Martínez et al., 2011; Kolb et al., 2015; Woodward et al., 2014) and has immediate implications for interpreting and modelling extinct vertebrate growth.

Palaeognaths, the sister group to all other modern aves (neognaths), consist of large flightless birds such as the extinct moas and elephant birds, the extinct and extant ostriches, rheas, cassowaries and emus, and the small tinamous and flightless kiwis (Apterygiformes). Modern aves like kiwis are descendents of non-avian dinosaurs and bone growth characters may conserve phylogenetic signals and be used to reconstruct non-avian dinosaur growth patterns based on bone cortex similarities. Molecular evidence suggests Apterygiformes diversified in response to Pleistocene glaciation and today are comprised of between 5 and 11 species, all of which are at various levels of 'at risk' and declining population sizes (Burbridge et al., 2003; Robertson et al., 2011; Weir et al., 2016). Population decline is a result of several factors including habitat loss, invasive predators and slow growth rates (McLennan et al., 1996, 2004; O'Donnell et al., 2017; Sales, 2005). Protracted growth (extension of juvenile development phase) in palaeognaths is a life history characteristic shared among elephant birds, moas and, despite their small size, kiwis (Bourdon et al., 2009; McLennan et al., 2004; de Ricqlès et al., 2016; Turvey et al., 2005). Slow growth rates and flightlessness in kiwis may have developed in response to insular environments lacking major terrestrial predators (Bourdon et al., 2009; de Ricqlès et al., 2016; Turvey et al., 2005). However, slow growth rates in kiwis currently result in prolonged exposure during vulnerable life stages in early ontogeny to invasive terrestrial predators (McLennan et al., 2004). Thus, osteohistological examination can further illuminate growth patterns; information vital for conservation planning and mapping phylogenetic influences on bone growth (e.g. Legendre et al., 2014; Marín-Moratalla et al., 2013). Here, we describe hindlimb and forelimb intraskeletal variation in bone microstructure, including LAG counts, in two North Island brown kiwis (*Apteryx mantelli*) of known age and gender to accomplish several goals:

1. Establish intraskeletal growth mark count variation and potential deviations from known age.
   Inferring the ontogenetic age of extinct vertebrates requires consideration of intraskeletal inconsistencies in LAG counts within extant vertebrates. LAGs, and other cyclical growth marks, represent an annual cessation or slowing of appositional bone growth and are present in vertebrates requiring more than 1 year to reach adult size (Castanet et al., 1993, 2004; Köhler et al., 2012). The most complete LAG records in fossils are typically found in long bones, with quantification of maximum annual apposition rates quantified specifically from major weight-bearing bones such as the tibia or femur (e.g. Padian et al., 2013; Stein & Sander, 2009). However, establishing optimal bones for age and growth rate quantification requires further testing and confirmation in modern taxa (Woodward et al., 2013). Due to variable remodelling rates, LAG counts can vary both intraskeletally and along the length of a single bone, complicating ontogenetic age assessment of extinct taxa given fossil preservation biases, incomplete material and institutional limitations on 'destructive' sampling (e.g. Cullen et al., 2014; Horner et al., 1999; Hübner, 2012; Werning, 2012). Rates and extent of medullary cavity expansion, cortical drift and secondary remodelling also vary intraskeletally and are influenced by biomechanical, pathological, physiological and ecological factors (Enlow, 1963; Padian, 2013; Padian et al., 2016; Skedros et al., 2003). Therefore, intraskeletal sampling provides insight into the extent of remodelling processes, cortical drift and ideal sampling locations for ageing and assessing growth. A previous report on bone microstructure in several species of kiwi noted the presence of LAGs in femora, tarsometatarsi and tibiotarsi, and extensive remodelling in tarsometatarsi and tibiotarsi, but precise details of intraskeletal LAG variation were absent (Bourdon et al., 2009).

Additionally, the maximum number of LAGs observed in a specimen is often referred to as the 'minimum age at death', recognizing potential discrepancies between maximum LAG counts and actual age (e.g. Kolb et al., 2015). Correlating absolute age and LAG counts is severely understudied due to, in part, insufficient age data in modern vertebrate museum collections. Tracking age in wild individuals requires intense observation, capture-mark-recapture and tagging: methods that may not be feasible for solitary or scarce taxa. Osteohistology may prove to be a useful tool in determining absolute age of salvaged kiwi; thus, providing essential data for population monitoring and conservation planning. A recent study on wild red deer of known age found cortical growth marks unreliable for accurate ageing (Calderon et al., 2019), but growth mark counts correlate with tooth eruption patterns, a well-documented technique for accurate ageing in mammals, in captive and wild *Addax nasomaculatis* and *Equus hemionus* (Marín-Moratalla et al., 2013; Nacarino-Meneses et al., 2016). Similar studies are lacking in modern aves, and an alternative ageing technique counting periosteal and endosteal lamellae in birds of known age has proven controversial (e.g. Broughton et al., 2002; Klomp & Furness, 1992). Sampling captive individuals with extensive life history data, including age at death, is ideal for studying the accuracy of cortical growth marks for ageing. Our study tests LAG count accuracy utilizing two captive *A. mantelli* of known age. Establishing ideal bone sampling locations for quantifying age, relative to known age and growth rates in these brown kiwi specimens will assist targeted bone sampling for establishing baseline life history data vital for conservation planning, as well as to expand the foundational extant bone database so that selection of specific fossil bones for histological analyses is validated.

2. Sex-specific bone microstructure characteristics
   Histological sampling of non-avian dinosaurs (hereafter, simply 'dinosaurs') revealed the presence of sex-specific medullary bone in both saurischians and ornithischians (e.g. Hübner, 2012; Lee & Werning, 2008; Schweitzer et al., 2005, 2016). Medullary bone remains the only character to confirm female sex in dinosaurs despite numerous attempts in identifying sexual dimorphism in dinosaurs (see Mallon, 2017 and references therein). Our sample presents the opportunity to analyse differences in cortical bone microstructure between sexes for use in exploring potential sex-specific markers in dinosaur cortical bone. Cortical signals of sex can also assist in identifying sex among modern museum specimens or salvaged wild individuals lacking sex-specific morphological characters, an important utility in using such specimens for assessing wild species population structure and dynamics.
3. Contributions to a broad database of vertebrate bone tissue descriptions.
   Life history interpretations from fossil taxa bone microstructure rely on modern bone microstructure descriptions and detailed surveys of modern tissue organization can reveal behavioural correlates with specific bone tissue types (e.g. Padian, 2013). For example, recent descriptions of mammalian bone tissue organization suggest a potential link between the presence of secondarily deposited CCCB and fossoriality (Heck et al., 2019; Legendre & Botha-Brink, 2018). Ecological and life history correlates in tissue organization also lend to conservation planning for related, threatened or difficult to study species using osteohistological descriptions (Heck et al., 2019; Marín-Moratalla et al., 2013). Moreover, detailed descriptions are important foundational works necessary for future hypothesis testing.

To accomplish these objectives, we provide comprehensive descriptions of tissue organization, vascularity and growth marks in the appendicular skeleton of the previously undescribed *A. mantelli*. Our study also incorporates forelimb sampling in addition to hindlimb skeletal elements. Finally, the specimens in our sample are of known age and sex, and detailed life history data are available for the female kiwi.

2 | MATERIALS

A captive-bred male and female North Island brown kiwi (*A. mantelli*) with recorded life history details were obtained by H.N.W. through arrangements with Kathy Brader, Brown Kiwi Species Survival Program Chairperson for N. Am/EU, and with U.S. Fish and Wildlife Service import permit number 130066. The male kiwi died of natural causes at the age of 14 years, 4 months. The female died at the age of 5 years, 4 months due to post-egg-laying complications. The female specimen was in the second year of egg production; breeding history was unavailable for the male kiwi. Captive male kiwis typically reach sexual maturity at 2 years and 3 months (Kiwi Captive Management Advisory Committee, 2004), therefore, we assume the male kiwi had reached sexual maturity as well. Both specimens were subjected to zoo necropsies and subsequently frozen prior to being shipped to Oklahoma State University—Center for Health Sciences, Tulsa, OK, USA, for study. The female kiwi was skeletonized upon arrival, whereas the male kiwi was first prepared for diffusible iodine-based contrast-enhanced CT (diceCT) using standard methodology (see Supporting information 1 for complete details) for a separate study. The male kiwi was destained prior to histological processing. Left and right femora, tibiotarsi, tarsometatarsi, humeri, ulnae and radii from each bird were histologically sampled. Generally, larger weight-bearing bones, such as femora, tibiotarsus and tarsometatarsus, preserve a more complete record of higher apposition rates and can be used to assess annual body mass increases (e.g. Campione & Evans, 2012; Klein & Sander, 2007; Padian & Lamm, 2013; Sander & Andrassy, 2006; Stein & Sander, 2009). However, very little to no histological descriptions of palaeognath forelimb bones have been published. Forelimb histology has previously been examined in ostrich and emu to analyse the correlation of bone tissue organization and absolute growth rates, and, in a separate study, the effects of biomechanical loading on forelimb bone cortices (Castanet et al., 2000; Kuehn et al., 2019). Prior to histological processing, the

male kiwi bones were unusually pliable along the longitudinal axis; the mid-diaphyses bent with slight pressure. Preliminary CT scans, prior to iodine-based preparation, suggest diminished mineralization in the male kiwi bones (T. L. Green, Pers. Obs.), but we cannot discount that diceCT preparation or destaining may have had a role in increased pliability (see Early et al., 2020).

3 | METHODS

Two serial transverse sections were produced from the mid-diaphysis from limb elements (Figure 1). The cortices of long bones are thicker at the area of minimum circumference and typically undergo less cortical remodelling relative to the remaining shaft and preserve a more complete record of growth (Sander & Andrassy, 2006). Additionally, the occurrence of calcified cartilage, metaphyseal bone and effects of processes such as trochanters is more limited at the midshaft relative to other regions along the length of the bone; cortical bone growth marks are less likely to be altered at the midshaft than in regions of the metaphysis or muscular processes (Padian et al., 2013). Longitudinal sections were produced from the diaphysis of left femora, tibiotarsi and tarsometatarsi of both specimens (Figure 1). Longitudinal sections of forelimb bones were unattainable due to limited material availability from such small bones. Longitudinal sections are used for confirming tissue identifications made from transverse sections (see Faure-Brac et al., 2019; Stein & Prondvai, 2014). Specimen chemical processing and ground section preparation followed protocol for extant undecalcified bone in Schweitzer et al. (2007). All sections were stained with toluidine blue at the Woodward Ballard Paleohistology Lab at Oklahoma State University-Center for Health Sciences to enhance contrast of cement lines and LAGs. Bone microstructure descriptions follow standard terminology of Enlow (1963), Francillon-Vieillot et al. (1990) and Huttenlocker et al., (2013) (but see Stein & Prondvai, 2014 and Prondvai et al., 2014) and hindlimb myology is derived from McGowan (1979). Figures and additional images available at morphobank.org (P4029).

4 | RESULTS

Osteohistological descriptions are organized by specimen (the female skeleton is described first) to allow for direct comparison of growth mark counts throughout each skeleton.

4.1 | Female Kiwi

4.1.1 | Femur

Tissue that is morphologically consistent with medullary bone (hereafter, simply 'medullary bone') extends into the medullary

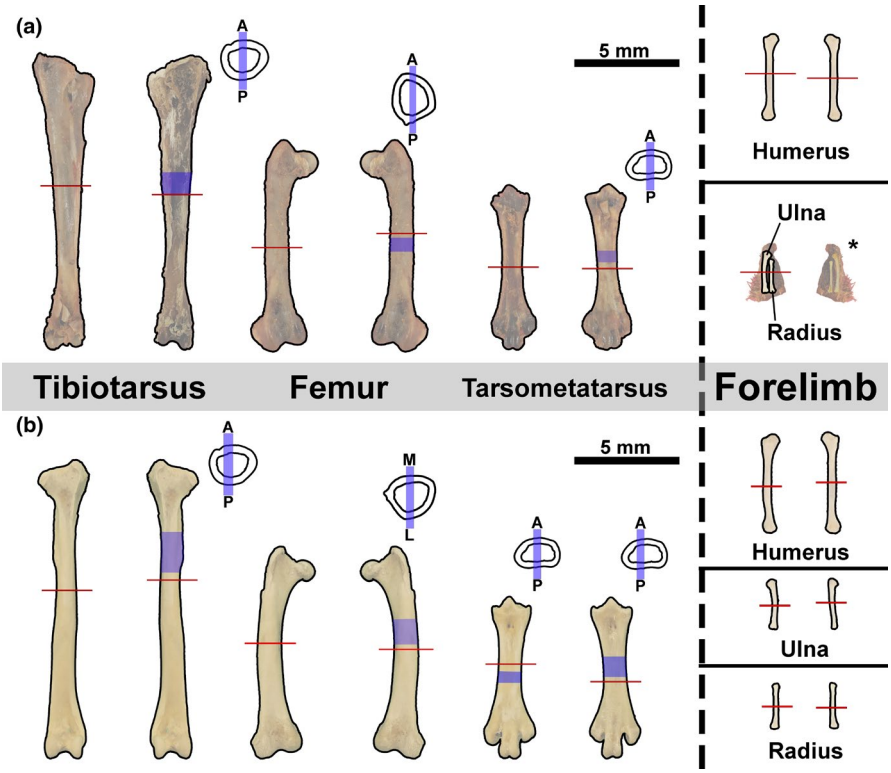

FIGURE 1 Cut-line locations. Transverse sections (red lines) taken, approximately, from the mid-diaphysis of (a) male kiwi and (b) female kiwi hindlimb and forelimb element. Longitudinal sections taken from each left hindlimb element diaphysis (blue shading). Longitudinal sections were either taken along medial-lateral axis or anterior-posterior (see blue bars on simplified cross sections)

cavity from the endosteal bone within the female kiwi's left femur (Figure 2a; see Canoville et al., 2019a, 2019b for medullary bone description). The endosteal layer of the female kiwi's left femur is composed of a thin band of transversely oriented avascular lamellar tissue, and was undergoing active resorption at the time of the animal's death. The endosteal layer is thickest on the postero-medial side near the attachment region of *m. adductor longus brevis* and thinnest around the antero-medial side. A single spicule of trabecular bone, composed of an outer border of lamellar endosteal tissue around an interior of woven bone, extends into the medullary cavity towards the antero-lateral side from the antero-medial side. The mid-cortex is composed of longitudinally oriented parallel-fibered tissue with regional shifts to transverse orientation and remodelled woven tissue. The remodelled woven tissue with secondary

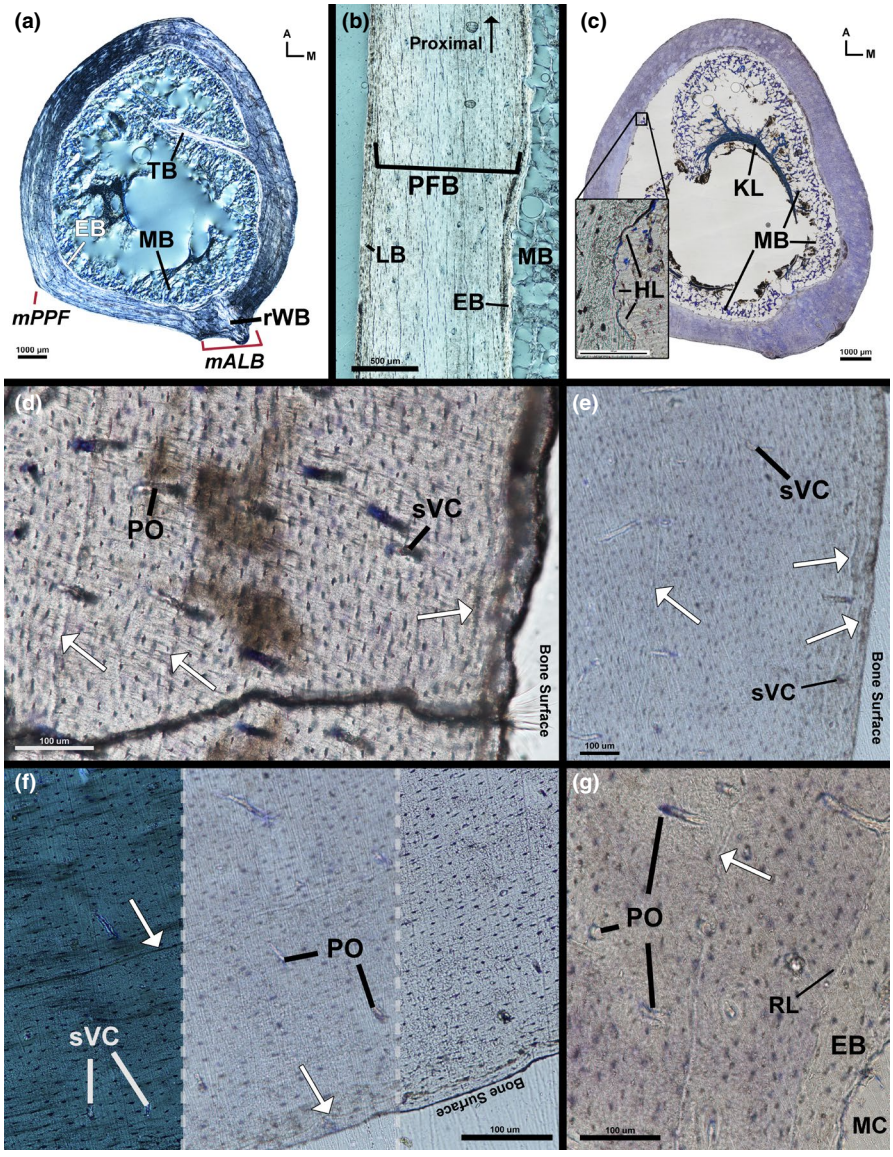

FIGURE 2 Female kiwi femora microstructure. (a) Transverse section of left femur under circular polarized light showing highly birefringent endosteal lamellar bone and remodelled woven bone in the poster-medial corner. (b) Longitudinal section of left femur medial diaphysis under circular polarized light. Mid-cortical parallel-fibered bone fibres are oriented parallel to section as indicated by elongated osteocyte lacunae. Osteocyte lacunae of outer cortical, transversely oriented, lamellar bone are plump and rounded. (c) Transverse section of toluidine stained right femur under linear light. Medullary bone extends off endosteal surface and attaches to a crescent-shaped Kastschenko's line within medullary cavity. Endosteal resorption is evident from multiple Howship lacunae (insert). (d) Three LAGs (arrows) are present on the medial side of left femur (imaged under linear light). (e) Three LAGs (one in the mid-cortex and two in the outer cortex) on the antero-medial side of the left femur (imaged under linear light). (f) Posterior side of right femur exhibiting LAG contrast under circular polarized light (left), linear light out of focus (centre) and linear light in focus (right). (g) Resorption line separates endosteal layer of lamellar bone and mid-cortical parallel-fibered bone. Arrows—LAGs, A—anterior, EB—endosteal bone, HL—Howship Lacunae, KL—Kastschenko's line, LB—lamellar bone, M—medial, mALB—*M. adductor longus brevis* attachment, MB—medullary bone, MC—medullary cavity, mPPF—*M. piriformis pars iliofemoralis* attachment, PFB—parallel-fibered bone, PO—primary osteon, RL—resorption line, rWB—remodelled woven bone, sVC—simple vascular canal, TB—trabeculae

osteons oriented longitudinally and radially composes the cortex on the postero-medial side where the attachment of *m. adductor longus brevis* is located (Figure 2a). Interestingly, a remodelled woven tissue complex is not present on the postero-lateral side where *M. piriformis pars ilio femoralis* attaches. Instead, the remaining mid-cortex is composed of longitudinally and transversely oriented parallel-fibered tissue. In longitudinal section, the mid-cortex is highly birefringent and osteocyte lacunae are flattened, confirming identifications from transverse views (Figure 2b). Vascular canals in the mid-cortex are typically simple vascular canals and vascular canals within primary osteons (Figure 2d); vascular orientation is longitudinal, radial or reticular. Generally, vascular canals on the medial side have a slight radial tilt, canals are reticular in the deep region of the mid-cortex on the lateral side and canals elsewhere are longitudinal. LAGs in the mid-cortex are extremely faint and cannot be fully traced around the circumference of the bone due to a lack of contrast. A maximum of three LAGs can be identified postero-medially in the transverse section of the left femur (Figure 2d), but LAGs could not be identified in the longitudinal section of the same bone (Figure 2b). The outer cortex of the left femur consists of a thin layer of transversely oriented, low vascular tissue ranging from lamellar to parallel-fibered around the circumference of the femur (Figure 2b). Several longitudinal vascular canals are located in the outer cortex (Figure 2e), which complicates labelling the outer cortex as an external fundamental system (EFS). Instead, the femur of the female kiwi appears to have been actively growing, albeit slowly, as it approached skeletal maturity.

The transverse section of the female kiwi's right femur mostly agrees with tissue and vascular composition described in the left femur. Medullary bone lines the medullary cavity side of endosteal bone and a condensation of tissue forms a crescent shape deep in the medullary cavity (Figure 2c). The tissue condensation stains partially blue with toluidine blue and is likely a Kastschenko's line (unresorbed mineralized embryonic tissue; see Francillon-Vieillot et al., 1990; Haines, 1942; Kastschenko, 1881) with medullary bone attached. The medullary bone extends off of the endosteum, contacts and condenses onto the Kastschenko's line. The Kastschenko's line may simply be a condensation of medullary bone as a Kastschenko's line is unexpected in a nearly skeletally mature individual. This study does not perform the necessary analysis to confirm either explanation. The endosteal layer is thin and displays local regions of lower birefringence in circular polarization, possibly due to collagen fibres oriented perpendicular to plane of section in these darker regions. The medullary border of the endosteal layer displays numerous Howship's Lacunae (Figure 2c), indicating endosteal resorption was ongoing at the time of death. The endosteal layer is separated from the mid-cortex by a resorption line (Figure 2g). The mid-cortex is longitudinally oriented parallel-fibered bone, and vascularity is oriented longitudinally, radially and, rarely, reticularly. The cortex near the *M. adductor longus brevis* attachment site is composed of longitudinally oriented parallel-fibered tissue with few secondary osteons and numerous primary osteons. The muscle attachment site is not as prominent possibly due to slight differences in the location of the section. Maximum LAG count in the transverse section of the right femur is three on the postero-medial side, similar to the left femur. Visibility is higher for a few LAGs in the right femur under circular polarized light (Figure 2f), but many of the LAGs remain difficult to discern.

4.1.2 | Tibiotarsus

The cortex of the left tibiotarsus has an endosteal layer of transversely oriented, avascular lamellar tissue (Figure 3a). The medullary border of the endosteal layer was being actively resorbed at the time of death; resorption was concentrated antero-medially. Similar to the right femur, medullary bone extends off of the endosteal layer into the medullary cavity to a potential Kastschenko's line (Figure 3a,c,d). The endosteal layer is separated from the mid-cortex by a resorption line indicating endosteal resorption of mid-cortical tissue occurred prior to deposition of endosteal lamellar bone. The mid-cortex of the left tibiotarsus is composed of heavily remodelled CCCB (Figure 3a). Some secondary osteons in the mid-cortex have longitudinally oriented tissue fibres resulting in a darker appearance in circularly polarized light. The mid-cortex of CCCB is thickest on the antero-lateral side and thinnest medially (Figure 3a). Mid-cortical CCCB is confirmed on the anterior and posterior sides in longitudinal section and appears as large interweaving fibre bundles (Figure 3c,d). The outer cortex is parallel-fibered tissue with longitudinally oriented simple vascular canals, vascular canals within longitudinally oriented primary osteons and vascular canals within secondary osteons (Figure 3e). Additionally, longitudinal sections of the tibiotarsus reveal numerous circumferentially oriented simple vascular canals within the outer cortex (Figure 3d). Collagen fibres of the outer cortex of parallel-fibered tissue increases in organization towards the periosteal surface; additionally, vascularity within the outer cortex decreases outward towards the periosteal surface. Decreasing vascularity and increasing collagen fibre organization suggest that formation of an EFS was in early development in the left tibiotarsus. Within the cortex are up to six possible LAGs (Figure 3e).

The mid-diaphyseal cortex of the right female tibiotarsus is similar to that of the left tibiotarsus. The medullary bone extends off the endosteal surface to a potential Kastschenko's line, similar to the right femur (Figure 3b). The endosteal layer is composed of avascular lamellar tissue oriented transversely with few regions of longitudinally oriented lamellar tissue. The mid-cortex is composed of remodelled CCCB and is thin on the medial side (Figure 3b). The outer cortex is composed of longitudinally oriented parallel-fibered tissue with simple vascular canals oriented longitudinally and vascular canals within longitudinally oriented primary osteons and, rarely, secondary osteons. The outer cortex is likely a developing, or incipient, EFS as in the left tibiotarsus. Very few secondary osteons impede into the outer cortex and, when present, are typically located internally in the outer cortex. Seven LAGs are found on the medial side of the right tibiotarsus (Figure 3f).

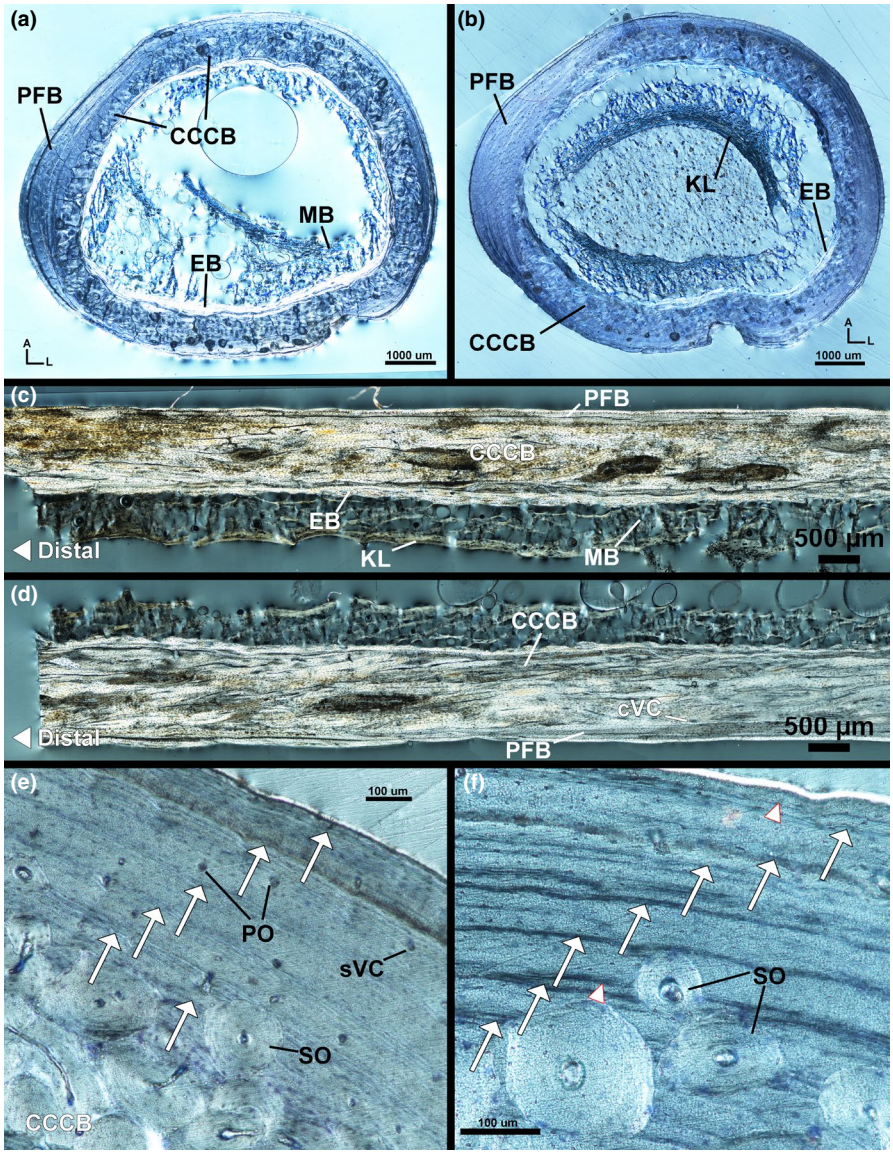

FIGURE 3 Female kiwi tibiotarsi microstructure. (a) Transverse section of left tibiotarsus under circular polarized light. The cortex is composed of endosteal bone, CCCB and parallel-fibered bone. (b) Transverse section of right tibiotarsus under circular polarized has similar composition as left tibiotarsus, but with distinct Kastschenko's line within medullary cavity. (c) Longitudinal section of posterior diaphysis from left tibiotarsus under circular polarized light. (d) Longitudinal section of anterior diaphysis from left tibiotarsus under circular polarized light. (e) Antero-medial corner of left tibiotarsus has inner mid-cortex of CCCB and outer mid-cortex and outer cortex of parallel-fibered bone with five LAGs. (f) Antero-medial corner of left tibiotarsus under circular polarized light has seven LAGs. Arrows—LAGs, A—anterior, CCCB—coarse compacted cancellous bone, cVC—circumferential vascular canal, EB—endosteal bone, KL—Kastschenko's line, L—lateral, MB—medullary bone, PFB—parallel-fibered bone, PO—primary osteon, SO—secondary osteon, sVC—simple vascular canal

4.1.3 | Tarsometatarsus

The mid-diaphysis of the female left tarsometatarsus has an endosteal layer of avascular lamellar tissue oriented transversely (Figure 4a). Medullary bone extends from the endosteal layer into the medullary cavity (Figure 4a). Medullary bone is not as prevalent in the tarsometatarsus as in the tibiotarsus or femur. The mid-cortex of the left tarsometatarsus is parallel-fibered tissue of varying organization and orientation with primary osteons and some secondary osteons. The anterior and posterior mid-cortex is composed of longitudinally oriented parallel-fibered tissue as confirmed by longitudinal sampling (Figure 4a,b). Vascularity in the anterior and posterior mid-cortex is longitudinally oriented simple vascular canals and canals within primary osteons with a few local regions of reticular vascularity. Secondary osteons, when present, are concentrated in the internal regions of the anterior mid-cortex. Tissue organization of the lateral and medial mid-cortex is loosely organized, transversely oriented parallel-fibered bone (Figure 4a).

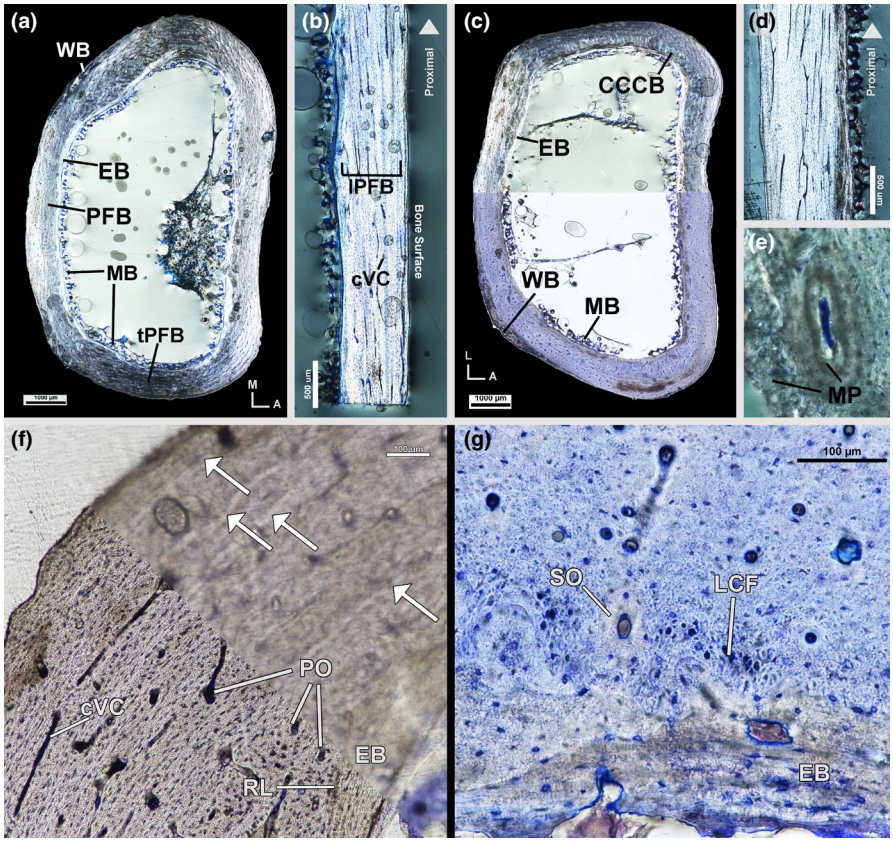

FIGURE 4 Female kiwi tarsometatarsi microstructure. (a) Transverse section of left tarsometatarsus under circular polarized light showing a cortex of endosteal bone, parallel-fibered bone and woven bone. (b) Longitudinal section of posterior diaphysis of left tarsometatarsus under circular polarized light with highly birefringent, longitudinally oriented, parallel-fibered bone. (c) Transverse section of right tarsometatarsus under circular polarized light (top) and linear polarized light (bottom). Cortex is similar to left tarsometatarsus with the addition of a small patch of CCCB on the antero-lateral side. (d) Longitudinal section of anterior diaphysis of right tarsometatarsus under circular polarized light showing highly birefringent parallel-fibered bone of the mid-cortex. (e) Metaplastic hard tissue is present at entheses in the left tarsometatarsus. (f) Antero-lateral left tarsometatarsus under linear polarized light in focus (bottom) and out of focus (top). Four LAGs are present with increased clarity when viewed out of focus. (g) Inner cortex of posterior right tarsometatarsus, stained with toluidine blue and imaged under linear polarized light, has large, longitudinal collagen fibre bundles in addition to lamellar endosteal bone and parallel-fibered mid-cortex. Arrows—LAGs, A—anterior, CCCB—coarse compacted cancellous bone, cVC—circumferential vascular canal, EB—endosteal bone, L—lateral, LCF—longitudinal collagen fibre bundles, lPFB—longitudinal parallel-fibered bone, M—medial, MB—medullary bone, MP—metaplastic tissue, PFB—parallel-fibered bone, PO—primary osteon, RL—resorption line, SO—secondary osteon, tPFB—transverse parallel-fibered bone, WB—woven bone

The lateral–medial axis was not longitudinally sampled and, thus, tissue organization in these regions cannot be confirmed in alternative orientations. Vascularity in the medial and lateral mid-cortex is primarily longitudinally oriented simple vascular canals and canals within primary osteons in addition to few circumferential canals and secondary osteons. Minimal remodelling has occurred throughout the cortex and secondary osteons, when present, are more prevalent postero-medially and postero-laterally. LAGs are difficult to identify; a total of four LAGs are present in the left tarsometatarsus (Figure 4f), but are not traceable around the entire circumference. The postero-medial and postero-lateral outer cortex is woven tissue (Figure 4a), likely formed in response to muscle attachments (e.g. *m. abductor digiti IV* attaches to the postero-lateral corner). The outer cortices at the entheses also contain tissue morphologically consistent with metaplastic hard tissue (sensu Horner et al., 2016; Figure 4e). Elsewhere, the outer cortex is longitudinally oriented parallel-fibered tissue with few vascular canals oriented longitudinally.

The right tarsometatarsus of the female kiwi was sectioned at the mid-diaphysis and varies slightly from the left tarsometatarsus in terms of mid-cortex tissue organization and vascularity, LAG count and remodelling. The mid-cortex of the right tarsometatarsus is composed of CCCB and parallel-fibered tissue (Figure 4c,d). CCCB composes the interior region of the mid-cortex on all sides, but is not present along the entire anterior or posterior sides (Figure 4c). The posterior mid-cortical vascularity of the right tarsometatarsus is primarily longitudinally oriented vascular canals in primary osteons, similar to the cortex of the left side. However, vascular orientation elsewhere consists of a mix of longitudinal, radial and reticular canals in primary osteons and very few circumferential vascular canals. Secondary osteon density is higher in the right tarsometatarsus with increased secondary osteons on the anterior and posterior sides. In

the right tarsometatarsus, the inner portion of the mid-cortex on the posterior side, where CCCB is absent, has a region of large, longitudinally oriented collagen fibres interrupted by secondary osteons (Figure 4g). A total of four LAGs are found in the cortex of the right tarsometatarsus.

4.1.4 | Humerus

The left and right humeri of the female are similar in tissue organization and vascularity at the mid-diaphysis. The humeri have an endosteal layer of transversely oriented avascular lamellar tissue (Figure 5a,b). The lamellar tissue was being actively resorbed along its endosteal surface at the time of the animal's death as evidenced by numerous Howship's lacunae along the endosteal surface (Figure 5b). The mid-cortex is remodelled parallel-fibered tissue with primary tissue fibres oriented transversely. A resorption line separates the endosteal layer and the mid-cortex indicating the endosteal side of the mid-cortex was resorbed prior to deposition of the endosteal lamellar tissue (Figure 5b). Vascularity in the mid-cortex is longitudinally oriented simple vascular canals and vascular canals within longitudinally oriented primary and secondary osteons. The

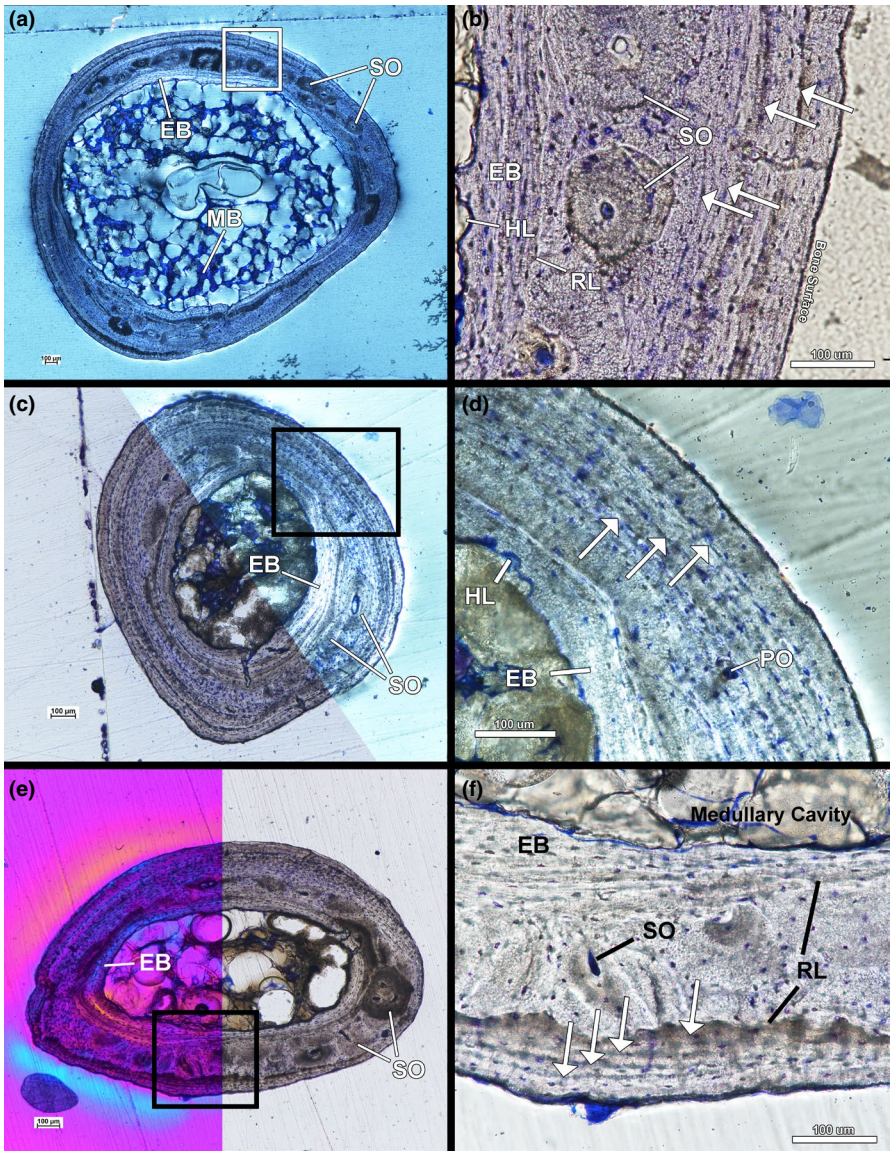

FIGURE 5 Female kiwi forelimb microstructure. (a) Transverse section of left humerus under circular polarized light showing endosteal lamellar bone, remodelled parallel-fibered bone and an outer cortex of parallel-fibered bone. (b) Four LAGs are found in the cortex of left humerus under linear polarized light. (c) Transverse section of left radius under linear polarized light (bottom) and circular polarized light (top). (d) Three LAGs can be found in the cortex of the radius (imaged under circular polarized light). (e) Transverse section of left ulna under a full lambda waveplate (left) and under linear polarized light (right). (f) The mid-cortex of the left ulna underwent resorption on the endosteal surface and periosteal surface prior to the deposition of endosteal bone and the outer cortex. The outer cortex has four LAGs at the mid-diaphysis. Arrows—LAGs, EB—endosteal bone, HL—Howship lacunae, MB—medullary bone, PO—primary osteon, RL—resorption line, SO—secondary osteon

secondary osteons are large and lamellar fibres are oriented longitudinally (SO appear dark in circularly polarized light and lacunae are round) (Figure 5a). There are four LAGs in the cortex of both humeri (Figure 5b). The outer cortex of the humeri has avascular longitudinal parallel-fibered tissue in addition to local regions of transversely oriented avascular lamellar tissue.

4.1.5 | Radius

The left and right radii of the female kiwi were sectioned at the mid-diaphysis and have an endosteal layer of avascular lamellar tissue that was being resorbed along the endosteal surface (Figure 5c,d). The mid-cortex of both radii is composed of parallel-fibered tissue primarily oriented transversely, but local shifts to longitudinal orientation occur. Few simple vascular canals oriented longitudinally and obliquely are present in the mid-cortex in addition to few secondary osteons (Figure 5c). The outer cortex is avascular lamellar tissue that shifts between transverse and longitudinal orientation around the bone and is interpreted as an EFS (Figure 5c). Three LAGs were found in the mid-cortex of both the right and left radii (Figure 5d).

4.1.6 | Ulna

The left and right ulnae have an endosteal layer of avascular, transversely oriented lamellar tissue undergoing resorption on the endosteal surface (Figure 5e,f). The mid-cortices of both ulnae are composed of remodelled, transversely oriented parallel-fibered tissue (Figure 5e). A resorption line separates the endosteal lamellar tissue from the mid-cortex in both ulnae. Mid-cortical vascularity is longitudinally oriented simple vascular canals and vascular canals within longitudinally oriented primary and secondary osteons (Figure 5e,f). The outer cortex of the ulna is EFS of avascular, transversely oriented lamellar tissue with local regions of longitudinal fibres, similar to the outer cortex of the female humeri. The longitudinal fibres are likely components of either parallel-fibered or lamellar tissue, but the ulnae were not longitudinally sectioned to confirm the tissue identification. The outer cortex is separated from the mid-cortex by a resorption line indicating the ulnae have undergone periosteal resorption prior to deposition of the EFS. Four LAGs were found in the outer cortex of both ulnae (Figure 5f).

4.2 | Male Kiwi

4.2.1 | Femur

The left femur of the male kiwi has a thin endosteal layer of avascular, transversely oriented lamellar tissue (Figure 6a). The endosteal layer is separated from the mid-cortex by a resorption line (Figure 6d). The mid-cortex of the left femur is composed of remodelled, transversely oriented parallel-fibered tissue (Figure 6a,b,d). Remodelling is less extensive in the mid-cortex on the anterior and antero-lateral sides; mid-cortical vascularity is, instead, vascular canals within longitudinally oriented primary osteons. Secondary osteon density in the mid-cortex increases along the medial and lateral side of the femur (Figure 6e); secondary osteon density peaks on the posterior side of the femur. Longitudinal sections show secondary osteon density also increasing distally on the anterior and posterior sides of the femur (Figure 6b). Few radial canals are present on the anterior side of the femur. The outer cortex of the left femur is an EFS of avascular lamellar tissue oriented transversely (Figure 6d). Few secondary osteons have invaded the outer cortex on the posterior, postero-medial and postero-lateral sides of the femur (Figure 6e). A maximum of three LAGs are present in the mid-cortex of the left femur and four additional LAGs are found in the EFS (Figure 6d).

The right femur of the male kiwi has an endosteal layer of avascular, transverse oriented lamellar tissue separated from the mid-cortex by a resorption line (Figure 6c). The mid-cortex of the right femur is composed of remodelled parallel-fibered tissue and remodelled CCCB. The collagen fibres of the parallel-fibered tissue are generally oriented transversely with local regions of longitudinal fibres. The interior of the antero-medial mid-cortex is CCCB separated from the external mid-cortical parallel-fibered tissue by a resorption line. Vascular canals within secondary osteons are oriented longitudinally and are most dense on the posterior side within the mid-cortex. Vascular canals within primary osteons are oriented longitudinal, circumferential and radially throughout the parallel-fibered component of the mid-cortex (Figure 6f,g). The right femur was cut at the level of a nutrient canal penetrating the cortex at the attachment site of *M. adductor longus brevis* (Figure 6c). The nutrient canal attachment site is surrounded by radially oriented, highly organized, parallel-fibered tissue as it penetrates through the cortex towards the medullary cavity, but the region of outer cortex in which the canal passes through is composed of longitudinally oriented lamellar tissue. The posterior edge is also the attachment site of *M. adductor longus et brevis*; tissue organization on the posterior side is likely the result of nutrient canal and muscle attachment site development. The outer cortex of the right femur is an EFS of avascular, transversely oriented lamellar tissue with regional shifts in organization to parallel-fibered tissue. There is a maximum of seven LAGs in the right femur: three LAGs in the mid-cortex and four LAGs within the EFS (Figure 6f,g).

4.2.2 | Tibiotarsus

The mid-diaphysis of the left tibiotarsus has a thin endosteal layer of avascular, transversely oriented lamellar tissue (Figure 7a). The endosteal layer is separated from the mid-cortex by a resorption line and the mid-cortex is composed of remodelled parallel-fibered

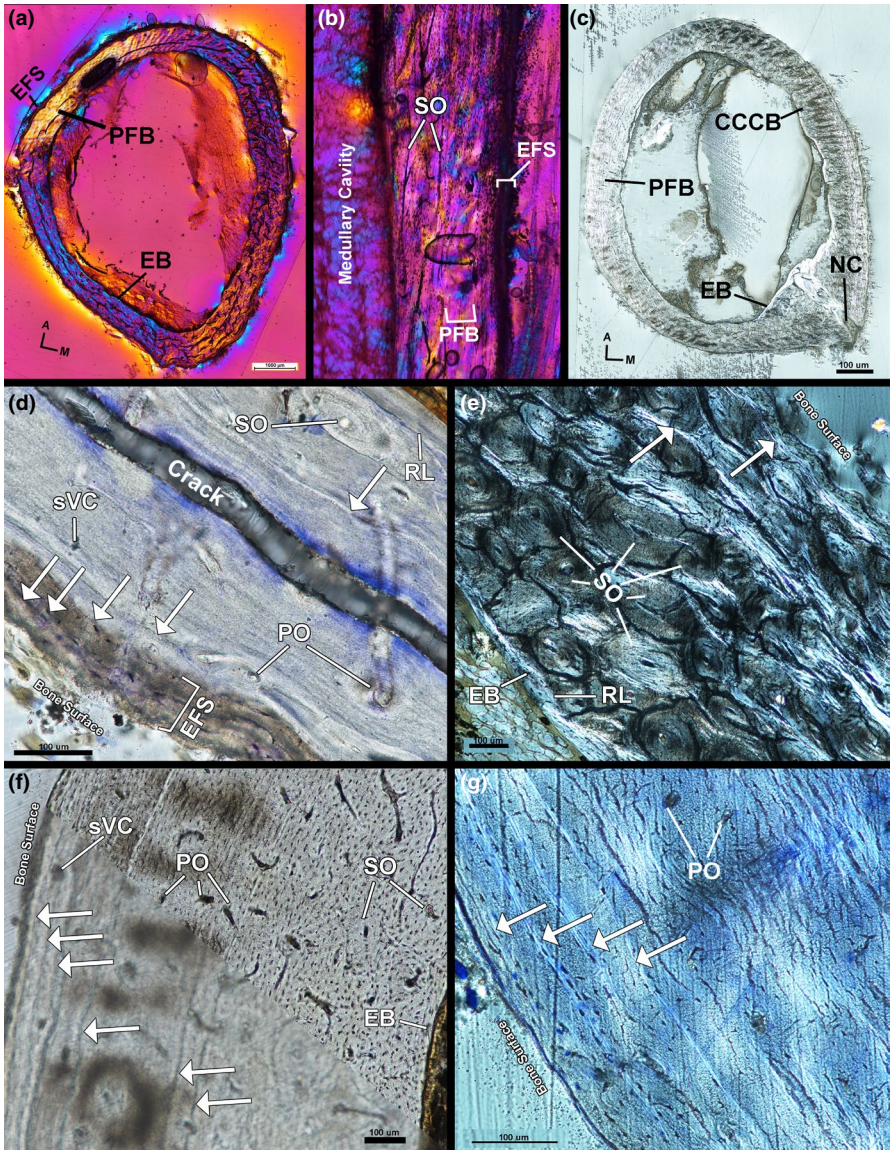

FIGURE 6 Male kiwi femora microstructure. (a) Transverse section of left femur under polarized light with full lambda waveplate. (b) Longitudinal section of left femur under polarized light with full lambda waveplate showing remodelled parallel-fibered bone in the mid-cortex. (c) Transverse section of right femur under circular polarized light. (d) Lateral side of left femur stained with toluidine blue and imaged under linear polarized light. Parallel-fibered bone composes the mid-cortex and an EFS forms the outer cortex. A total of five LAGs can be identified on the lateral side. (e) Cortex of left femur on medial side, imaged under circular polarized light, is heavily remodelled and only two LAGs can be located. (f) Antero-lateral side of right femur under linear polarized light out of focus (bottom) and in focus (top). Six total LAGs can be found and have higher contrast when viewed out of focus. (g) Postero-lateral cortex of right femur stained with toluidine blue under circular polarized light. Four LAGs are found in the outer cortex EFS on this side of the femur. A—anterior, Arrows—LAGs, CCCB—coarse compacted cancellous bone, EB—endosteal bone, EFS—external fundamental system, M—medial, NC—nutrient canal, PFB—parallel-fibered bone, PO—primary osteon, RL—resorption line, sVC—simple vascular canal, SO—secondary osteon

tissue; collagen fibres of parallel-fibered tissue are oriented transversely (Figure 7a,c–e). Vascularity in the mid-cortex consists of vascular canals within longitudinally oriented secondary osteons in addition to vascular canals within longitudinally and circumferentially oriented primary osteons (Figure 7e). The outer cortex of the left tibiotarsus is an EFS of avascular, transversely oriented parallel-fibered tissue with local regions of lamellar tissue (Figure 7c–e). Few secondary osteons are present in the EFS. The left tibiotarsus has two LAGs in the mid-cortex and three LAGs within the EFS.

The mid-diaphysis of the right tibiotarsus has a very thin endosteal layer of avascular lamellar tissue with transversely oriented fibres (Figure 7b,f–g). The endosteal layer is separated from the mid-cortex by a resorption line (Figure 7f). The mid-cortex of the right tibiotarsus is heavily remodelled, parallel-fibered tissue with longitudinally oriented simple vascular canals

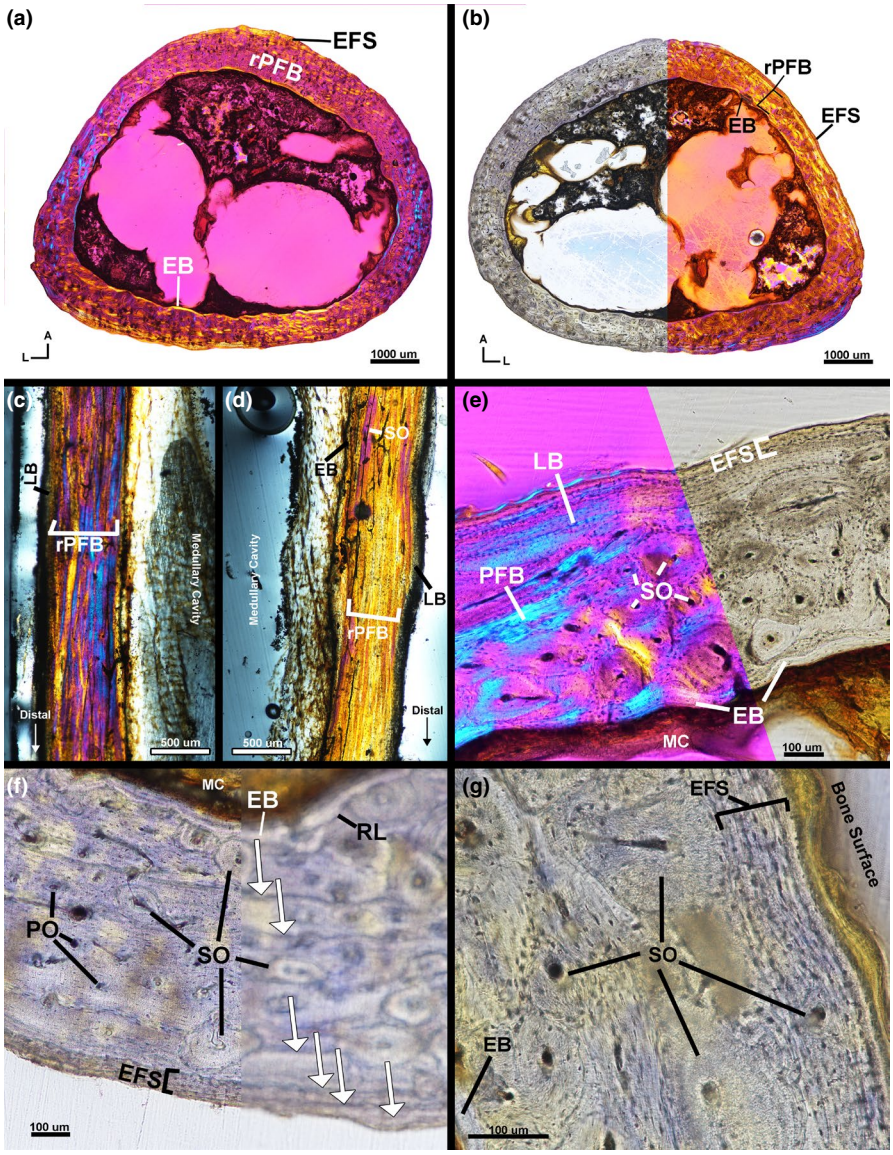

FIGURE 7 Male kiwi tibiotarsi microstructure. (a) Transverse section of left tibiotarsus under linear polarized light with a full lambda waveplate. (b) Transverse section of right tibiotarsus under linear polarized light without a waveplate (left) and with a full lambda waveplate inserted (right). (c) Longitudinal section of anterior diaphysis of left tibiotarsus under linear polarized light with full lambda waveplate. (d) Longitudinal section of posterior diaphysis of left tibiotarsus under linear polarized light with full lambda waveplate. (e) Lateral cortex of left tibiotarsus is composed of endosteal bone, remodelled parallel-fibered bone and an EFS. (f) Posterior cortex of right tibiotarsus under linear polarized light in focus (left) and out of focus (right). Six total LAGs are present on the posterior side in the mid-cortex of remodelled parallel-fibered bone and in the EFS. (g) Lateral side of right femur under linear polarized light showing the heavy remodelling in the mid-cortex and an EFS. A—anterior, Arrows—LAGs, EB—endosteal bone, EFS—external fundamental system, L—lateral, LB—lamellar bone, MC—medullary cavity, PFB—parallel-fibered bone, PO—primary osteon, RL—resorption line, rPFB—remodelled parallel-fibered bone, SO—secondary osteon

and vascular canals within longitudinal primary and secondary osteons (Figure 7b,f). Remodelling is less extensive on the postero-medial region. Parallel-fibered tissue of the mid-cortex is primarily oriented transversely with regional shifts to longitudinal orientation. The outer cortex is composed of an EFS of avascular, transversely oriented lamellar tissue with little remodelling (Figure 7b,f); secondary osteons are present in the outer cortex on the antero-medial and lateral sides (Figure 7g). The right tibiotarsus has three LAGs in the mid-cortex and three additional LAGs in the EFS (Figure 7f).

4.2.3 | Fibula

The right and left fibulae were also sectioned with the male tibiotarsi at the mid-diaphysis level of the tibiotarsi. Both fibulae were

entirely remodelled and composed of longitudinally oriented secondary osteons.

4.2.4 | Tarsometatarsus

The mid-cortex of the left tarsometatarsus is partially obstructed by unusually darkened regions (Figure 8a). The obstruction is likely the result of prolonged submersion in formalin solution. Regardless, an endosteal layer of avascular, transversely oriented lamellar tissue is visible but incomplete along the endosteal border of the cortex (Figure 8a,b). The endosteal layer is thickest on the posterior side of the tarsometatarsus and thinnest on the anterior side. The endosteal layer is separated from the mid-cortex by a resorption line. The mid-cortex, although partially obscured, is heavily remodelled parallel-fibered tissue with longitudinally oriented vascular canals within primary and secondary osteons (Figure 8a,b). Longitudinal sectioning reveals some variation in osteon orientation, but the majority of osteons are oriented longitudinally (Figure 8b). The extent of remodelling is difficult to discern due to obstructions, but remodelling appears concentrated on the posterior side. Anteriorly, the mid-cortical parallel-fibered tissue is oriented longitudinally as confirmed by longitudinal sectioning (Figure 8b). The mid-cortex parallel-fibered tissue is continuous with the outer cortex on the anterior, postero-medial and postero-lateral sides of the tarsometatarsus. The outer cortex of the medial, lateral and posterior sides is a thin layer of avascular lamellar tissue with few secondary osteons and is interpreted as an EFS. However, the external portion of the outer cortex of the postero-medial and postero-lateral side appears to have been torn and is absent (Figure 8a). Obstructions block LAG visibility in the mid-cortex, but a maximum of two LAGs are present in the outer cortex of the left tarsometatarsus on the anterior side (Figure 8d).

Regions of the endosteal layer and innermost cortex of the right tarsometatarsus are also partially obscured (Figure 8c). An endosteal layer of avascular, transversely oriented lamellar tissue is present in unobstructed areas and partially visible through the darkened obstruction. The endosteal layer and mid-cortex are separated by a resorption line indicating endosteal resorption of the

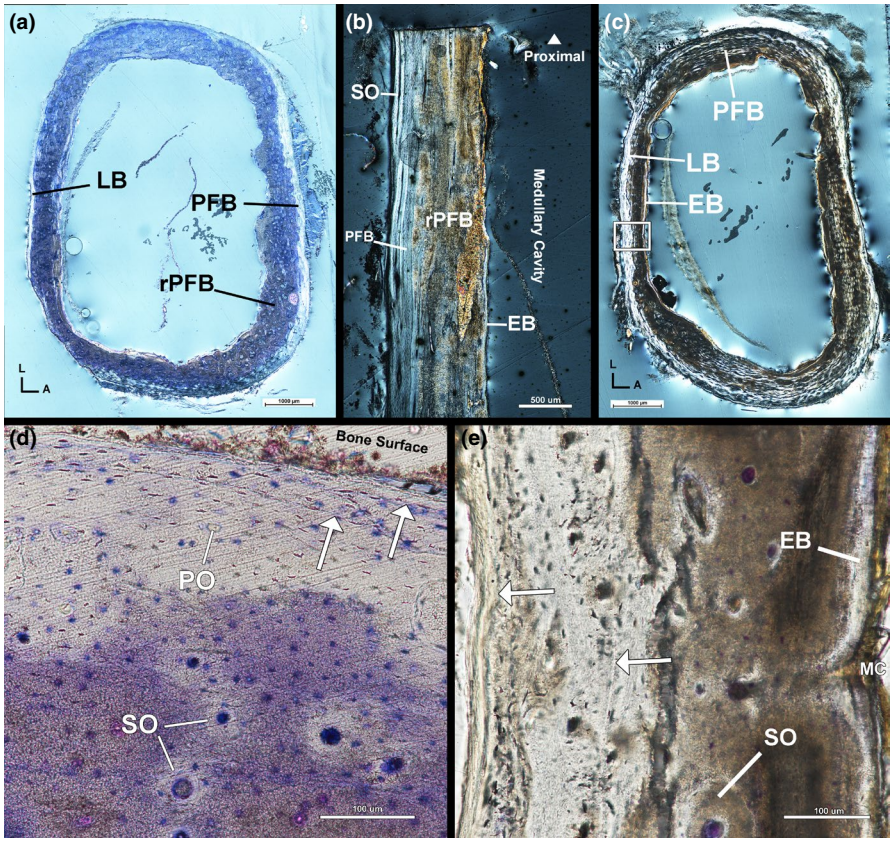

FIGURE 8 Male kiwi tarsometatarsi microstructure. (a) Transverse section of left tibiotarsus under circular polarized light. Cortex is mostly remodelled parallel-fibered bone and an outer cortex of lamellar and parallel-fibered bone. (b) Longitudinal section of left tarsometatarsus under circular polarized light confirming cortical composition described in transverse section. (c) Transverse section of right tibiotarsus under circular polarized light. (d) Antero-medial corner of left tibiotarsus under linear polarized light. Two LAGs are visible in this region of the left tibiotarsus. (e) Posterior side of right tibiotarsus under linear polarized light showing two LAGs: one in the outer cortex and one in the mid-cortex. A—anterior, Arrows—LAGs, EB—endosteal bone, L—lateral, LB—lamellar bone, MC—medullary cavity, PFB—parallel-fibered bone, PO—primary osteon, rPFB—remodelled parallel-fibered bone, SO—secondary osteon

mid-cortex occurred prior to deposition of the endosteal lamellar tissue. The mid-cortex is remodelled, vascular parallel-fibered tissue oriented transversely (Figure 8c). Primary parallel-fibered tissue is less remodelled on the lateral and medial sides. Vascular canals of the mid-cortex are contained within longitudinally oriented primary and secondary osteons (Figure 8e). The outer cortex is parallel-fibered tissue oriented transversely with little remodelling concentrated postero-medially. The outer cortex of the right tarsometatarsus is likely an EFS, although the tissue is less organized than in the left tarsometatarsus. The right tarsometatarsus has one LAG in the mid-cortex and one LAG within the outer cortex (Figure 8e).

4.2.5 | Humerus

The left humerus of the male kiwi was sectioned proximal to the mid-diaphysis, while the right humerus was sectioned at the mid-diaphysis (Figure 1). Both humeri have an endosteal layer of avascular lamellar tissue showing signs of resorption along the layer's endosteal border (Figure 9a). The endosteal layer is separated from the mid-cortex by a resorption line (Figure 9b). The mid-cortex of the humerus is entirely remodelled and, thus, composed of longitudinally oriented secondary osteons (Figure 9a,b). The outer cortex is avascular lamellar tissue and is separated from the mid-cortex by a resorption line (Figure 9b). A maximum of four LAGs are present in the outer cortex of the right humerus (Figure 9b), but LAGs could not be identified in the left humerus.

4.2.6 | Ulna/Radius

Removal of soft tissue from small fragile forelimb elements was difficult due to excess formalin fixation prior to skeletonization. The forearms of the male kiwi were embedded without skeletonizing and sectioned approximately at the mid-diaphysis, but section location could not be visually confirmed due to remaining soft tissues. The right forearm sections contained both the ulna and radius; however, the left forearm sections did not contain either bone. Therefore, we will only describe the right ulna and radius of the male kiwi. The right ulna and radius of the male kiwi are composed entirely of secondary osteons oriented parallel to the long axis of the ulna. LAGs were not visible in either of the male ulnae or radii (Figure 9c,d).

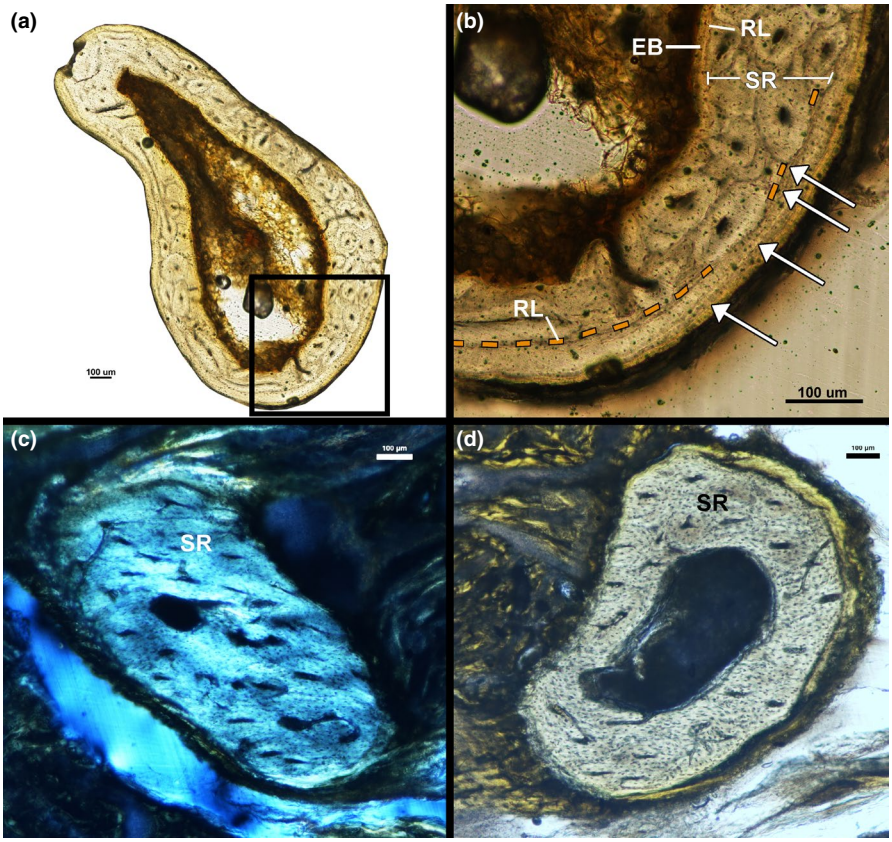

FIGURE 9 Male kiwi forelimb microstructure. (a) Transverse section of left humerus under linear polarized light. (b) Cortex of left humerus is composed of a thin layer of endosteal lamellar bone, mid-cortex of remodelled bone and an outer cortex of lamellar bone with four LAGs. (c) Transverse section of left ulna under circular polarized light. Ulna is composed entirely of remodelled tissue. (d) Transverse section of left radius under linear polarized light. Radius is composed entirely of remodelled tissue. Arrows—LAGs, EB—endosteal bone, RL—resorption line, SR—secondary remodelling

5 | DISCUSSION

5.1 | Variation in tissue organization

In general, bone tissue organization is best described as a spectrum from highly unorganized woven tissue to highly organized lamellar tissue, and tissue organization reflects rate of bone deposition (e.g. Amprino, 1947; Francillon-Vieillot et al., 1990). In agreement with Bourdon et al. (2009), primary tissue organization in the long bones of the male and female North Island Brown Kiwi is parallel fibered, interrupted by cyclical growth marks, and with mostly longitudinal vascular canals within primary and secondary osteons. Cortical primary organization increases and cortical vascularity decreases from the innermost cortex to the periosteal surface in both kiwis. Primary osteons within male and female cortices exhibit few lamellae and osteocyte lacunae, potentially fitting loose definitions of 'incipient primary osteons' (Woodward et al., 2014). Neither kiwi exhibited sexually dimorphic cortical tissue organization or vascularity, with the exception of medullary bone within the medullary cavity of female hindlimb elements. Thus, skeletal growth patterns in the kiwi consist of cyclically deposited parallel-fibered tissue with decreasing vascularity through ontogeny, a departure from typical avian bone which consists of uninterrupted, rapidly deposited woven tissue (Bourdon et al., 2009).

Modern and fossil aves are severely under-represented in osteohistological descriptions (Wood & de Pietri, 2015). Histological descriptions have been completed for relatively few avian taxa such as Charadriformes (Smith & Clarke, 2014), Anseriformes (e.g. Marsà et al., 2019), Sphenisciformes (e.g. Cerda et al., 2015), Palaeognaths (e.g. Turvey et al., 2005) and several basal forms such as *Hesperornis* and *Ichthyornis* (Chinsamy et al., 1998; Wilson & Chin, 2014). These previous investigations have revealed a shared growth strategy among most ornithurines, including most palaeognaths, in which fibrolamellar tissue is rapidly deposited followed by the deposition of an EFS, or outer circumferential layer (OCL), with the attainment of skeletal maturity. However, kiwi bird limb bone growth strays from this general pattern. Instead, appositional growth is much slower throughout the individual's life, as indicated by cyclical parallel-fibered tissue, which is similar to patterns found in some Enantiornithines (e.g. Chinsamy et al., 1995). Similar to most ornithurines, and indeed most vertebrates, skeletal maturity in the kiwi was represented by an EFS (or OCL) of avascular lamellar and parallel-fibered tissue (e.g. Ponton et al., 2004; Woodward et al., 2013). Slow, protracted growth over many years is unique among most ornithurines, and in the kiwi bird is likely due to a combination of (1) the kiwi's low basal metabolism relative to other aves and (2) environmental factors such as limited resources and the historical absence of large predators in New Zealand (Bourdon et al., 2009; McLennan et al., 2004). We review each factor in turn: (1) Bone tissue organization and vascular density/orientation directly reflect growth rate which is correlated with physiological parameters such as metabolic rates (Amprino, 1947). Relatively high growth and metabolic rates in most modern aves result in bone cortices composed of fast-growing fibrolamellar tissue (e.g. Turvey et al., 2005). Kiwi has notably lower metabolic rates relative to most modern aves (Calder & Dawson, 1978; McNab, 1994); lower metabolic rate and lower growth rates result in slower forming parallel-fibered tissue in the kiwi bone cortices. (2) Vertebrates with high growth rates lower certain predation risks based on body size attainment alone, but high growth rates also require high energetic demands and resource consumption. The kiwi evolved in resource-limited environments devoid of large nocturnal predators (Holdaway et al., 2001; Lee et al., 2001). McLennan et al. (2004) suggest the absence of predators allowed kiwi life history to freely develop in order to minimize energy requirements, thus, resulting in protracted growth, extreme precociality, small size and reduced metabolic rates.

Parallel-fibered tissue in kiwi cortices appears to be a reflection of growth and physiology, but behaviour and biomechanical function are also represented in the form of a peculiar tissue type: CCCB. CCCB is formed by osteoblast activity depositing new tissue along the endosteal margins of trabeculae resulting in the infilling of empty space between trabecular struts (Enlow, 1963). The overall process of CCCB formation transforms cancellous bone into compact bone and typically occurs during cortical drift. CCCB is a peculiar tissue and has been described in a variety of taxa including armadillos (Heck et al., 2019), aardvarks (Legendre & Botha-Brink, 2018), wombats (Walker et al., 2020), rodents (Garrone et al., 2021; Montoya-Sanhueza & Chinsamy, 2017) and some non-avian dinosaurs (e.g. Avrahami et al., 2019; Woodward et al., 2018), although some authors note that CCCB is difficult to identify and may be more widespread throughout vertebrate cortical tissue than originally thought (Heck et al., 2019). Nonetheless, CCCB is currently hypothesized to be indicative of fossorial behaviour to some degree and has been used to infer fossorial behaviour in orodromine non-avian dinosaurs, although the link between behaviour and tissue type is complex (Avrahami et al., 2019; Legendre & Botha-Brink, 2018). CCCB in the cortices of the kiwi, although sparse and inconsistent in location, provides another example of a link between this particular tissue and fossorial lifestyles; kiwis utilize their hindlimbs in the construction of numerous burrows across their home range and in scratch digging during foraging, similar to behaviours observed in the nine-banded armadillo (Sales, 2005).

In addition to influences stated previously, tissue composition in modern birds and some non-avian dinosaurs is also influenced by a sex-specific behaviour: egg laying. Medullary bone is formed in female birds during the egg-laying cycle as a calcium reservoir, and confirmation of its identification is highly dependent on chemical analyses (Schweitzer et al., 2016). This tissue forms in the medullary cavity of female birds along the endosteal margin of the cortex and is typically woven in organization and highly vascular (e.g. Canoville et al., 2019a, 2019b; Werning, 2018). Medullary bone has been identified in some non-avian dinosaurs and is currently the only reliable method of extinct dinosaur sex determination (Bailleul et al., 2019 and references therein). However, observation of medullary bone in modern or fossil specimens is highly dependent on the timing of an animal's death as medullary bone is resorbed and catabolized

for eggshell formation. In the current study, the female kiwi died of complications shortly after an egg-laying event and medullary bone is found in the hindlimb cortices of the female kiwi. The distribution of medullary bone appears to decrease distally among femora, tibiotarsi and tarsometatarsi and distally within each element as observed in longitudinal sections. Werning (2018) used a candling method to describe the distribution of medullary bone across modern avian groups and described medullary bone in the humerus, femur and tibiotarsus of the kiwi. Additionally, Canoville et al. (2019a, 2019b) investigated the extent of intraskeletal medullary bone across aves and observed consistent presence of medullary bone in the *Rhea* and Tinamidae ulnae and radii. Medullary bone was not found in the forelimbs of the female kiwi in the current study, and more rigorous chemical processing is necessary to fully describe the presence and intraskeletal distribution of medullary bone in kiwis generally.

5.2 | LAG Count Variation

Lines of arrested growth are used to assess absolute age, skeletal maturity and sexual maturity in extant and extinct vertebrates (see Woodward et al., 2013). In turn, ageing extinct vertebrates allow further analyses of population structure dynamics, heterochrony and intraspecific variation in growth rates. Life history reconstruction relies on accurate ageing techniques, but processes such as medullary cavity expansion, cortical remodelling and periosteal resorption can obliterate cortical growth marks vital for accurate ageing (Woodward et al., 2013). Intraskeletal sampling of modern vertebrates of known age is necessary for establishing optimal sampling locations for ageing and potential differences between known age and LAG count (e.g. Castanet et al., 2004). Here, North Island brown kiwi exhibits intraskeletal variation and LAG count variation in relation to known age (Table 1).

TABLE 1 Counts of lines of arrested growth identified in each skeletal element of the male and female *Apteryx mantelli*

Skeletal element	Female (5 years old)	Male (14 years old)
Left femur	3	7
Right femur	3	7
Left tibiotarsus	6	5
Right tibiotarsus	7	6
Left tarsometatarsus	4	2
Right tarsometatarsus	4	2
Left humerus	4	–
Right humerus	4	4
Left radius	3	–
Right radius	3	–
Left ulna	4	–
Right ulna	4	–

The 14 year-old male kiwi has extensive remodelling, medullary cavity expansion and periosteal resorption that likely obliterated numerous LAGs in all sampled skeletal elements. Regardless, large, weight-bearing hindlimb elements contain the highest number of observable LAGs: both femora have seven LAGs and tibiotarsi have a maximum of six LAGs. Tarsometatarsi, fibulae and forelimb elements have higher levels of resorption and remodelling and, thus, have lower LAG counts and are, therefore, likely unreliable age indicators in older kiwis. The 5 year-old female kiwi has far less remodelling in all skeletal elements. Forelimb and hindlimb elements have three to four LAGs, with the exception of six to seven LAGs in the tibiotarsi. The large disparity in LAG count between the tibiotarsi and other skeletal elements may indicate a delayed onset of extensive cortical remodelling and obliteration of previously formed LAGs in the tibiotarsi, but a more comprehensive ontogenetic sample is required to test this hypothesis.

LAG count varied from known age in both specimens. Remodelling likely obliterated previously deposited LAGs in the male kiwi long bones, but a more extensive ontogenetic series is needed to confirm remodelling processes. Still, a decoupling of age and LAG deposition after attainment of skeletal maturity is supported by our observations of the 14-year-old male kiwi and is consistent with observations of wild red deer (Calderon et al., 2019) and captive mouse lemurs (Castanet et al., 2004). *Apteryx mantelli* skeletal maturation is obtained at approximately 4.5–6 years of age followed by low rates of periosteal bone deposition, typically resulting in an EFS (Beale, 1985, 1991; Bourdon et al., 2009). LAG counts within the EFS of the 14-year-old male kiwi reach a maximum of four in the mid-diaphysis of the femur; eight to ten LAGs would be expected in the EFS given tight coupling between age and LAG deposition. The 5-year-old female kiwi also has, generally, lower cortical LAG counts relative to age, likely a result of LAG obliteration due to medullary cavity expansion. Curiously, the female tibiotarsi have six to seven LAGs: five to six within the cortex and one LAG in the EFS. Intraskeletal disparity in LAG counts may also be a reflection of increase resource availability or artificial photoperiodicity (see Castanet et al., 2004) in captivity and not a true representation of wild kiwi growth mark deposition (Prier et al., 2013).

Bone growth marks are formed in correlation with unfavourable seasons or events interrupting normal bone growth (e.g. Köhler et al., 2012; Nacarino-Meneses & Köhler, 2018). For example, weaning lines have been observed in bone cortices of some mammals (e.g. Morris, 1970; Nacarino-Meneses & Köhler, 2018) and hatching lines have similarly been described in reptiles (e.g. Hugi & Sánchez-Villagra, 2012), amphibians (e.g. Bruce & Castanet, 2006) and archosaurs (e.g. Rogers et al., 2016). Bone growth mark morphology varies and can be a distinct zone of tissue or a distinct hypermineralized line, as in a LAG (see Francillon-Vieillot et al., 1990; Klevezal, 1996; Woodward et al., 2013 and references therein). LAGs are typically formed annually (e.g. Castanet et al., 2004; Köhler et al., 2012), although the presence of 'double-LAGs' or 'triple-LAGs' in vertebrate long bone cortices is likely a sign of some developmental plasticity (e.g. Klein et al., 2019). Starck and Chinsamy (2002) examined cortical bone response, including LAG

formation, to variable environmental conditions on the Japanese quail (*Coturnix japonica*). The authors implemented food limitations and biomechanical loading to separate experimental groups of *C. japonica*, but neither environmental condition induced the formation of annuli, LAGs or other growth marks. Excess LAGs in the bone cortices of the kiwi, in addition to the results of Starck and Chinsamy (2002), indicate plasticity in LAG formation is complex and require further investigation. The innermost growth mark in the female kiwi may be a hatching line explaining the discrepancy between LAG count and actual age. However, the innermost LAG is morphologically similar to other LAGs within the cortex of the tibiotarsi. Alternatively, the presence of excess LAGs within bone cortices of the female *A. mantelli* could be the cessation of growth correlating with late stages of egg development.

Egg production is a massive undertaking for kiwi; additional energy expenditures equivalent to near 100% of the female kiwi's basal metabolic rate are required during the period of egg production (Prinzinger & Dietz, 2002). An average North Island brown kiwi weighs approximately 2.2 kg and lays an egg around 416 g, an egg weight 400% higher than expected relative to body mass (Prinzinger & Dietz, 2002; Sales, 2005). Egg production and laying results in significant weight loss in female North Island brown kiwis (Potter et al., 1996). Appositional bone growth may slow or halt during this period as resources and energy are focused and mobilized for egg production. Formation of a LAG in response to egg laying would be a sexually dimorphic signal within the bone cortices with potential utility in determining sex in extinct archosaurs. Our current investigations cannot confirm this potential dynamic, but more intensive ontogenetic sampling may resolve such a hypothesis. Regardless, excess number of LAGs in the kiwi cortices is evidence of plasticity in LAG formation, although excess LAGs may be a product of artificial conditions in captive rearing. Studies examining cortical growth marks in wild individuals of known age are necessary to confirm our results because these findings have widespread implications on previous, and future, skeletochronological analyses in fossil taxa.

5.3 | Implications for extinct taxa

Growth marks in extinct dinosaurs, both avian and non-avian, are used to assess ontogenetic changes, sexual maturity and skeletal maturity (see Bailleul et al., 2019; Padian & Lamm, 2013 and references therein). Construction of non-avian dinosaur growth curves relies heavily on cortical bone growth marks (e.g. Woodward et al., 2015) and, often, the assumption of minimal intraskeletal variation. Intraskeletal variation has often been ignored as a potential source of error due to (1) a lack of foundational intraskeletal examinations such as this study; (2) the scarcity of the fossil record and (3) limitations on specimen availability for histological sampling. For example, Erickson and Tumanova (2000) constructed growth curves for the ceratopsian *Psittacosaurus mongoliensis* using growth marks from fragmented samples of humeri, femora and tibiae. Potential intraskeletal variation in *P. mongoliensis* would lead to inaccurate growth curves and possibly misleading inferences of other fossil taxa. Here, intraskeletal growth mark variation in the kiwi highlights the need for consistency in skeletal element sampling for quantitative analyses and interpretations.

Numerous intraskeletal examinations of non-avian dinosaur taxa suggest skeletal elements with limited medullary cavity expansion, such as weight-bearing limb bones, contain the highest number of growth marks (e.g. Cullen et al., 2014; Horner et al., 1999). The large hind limb elements of the kiwi contain the highest number of growth marks, similar to growth mark variation found in some mammals (e.g. García-Martínez et al., 2011; Sander & Andrassy, 2006) and non-avian dinosaurs (e.g. Horner et al., 1999). The cortex of the kiwi fibulae does not contain any growth marks, is composed entirely of remodelled tissue and has limited expansion of the medullary cavity. Similarly, non-weight-bearing bones of the forelimb were composed primarily of remodelled tissue and LAG counts lower than those found in the hindlimb elements and support hypotheses stated in Padian et al. (2016) that remodelling in reduced forelimbs is likely a manifestation of metabolic processes rather than a biomechanical response due to minimal usage (Padian et al., 2016). Our findings provide more support for the use of large weight-bearing limb bones in examining skeletochronology of extinct dinosaur taxa.

Skeletal maturity can be assessed histologically by the presence of an EFS lining the outer bone cortex. An EFS is composed of avascular, slowly deposited tissue such as parallel-fibered bone or lamellar bone and is the result of drastic reductions in bone apposition. Cortical primary tissue can transition into an EFS or can be delineated from the outer EFS by a periosteal resorption line. The presence of an EFS within a single bone cortex indicates the attainment of maturation for that specific bony element. However, each skeletal element has its own ontogenetic trajectory and each bone varies in timing of maturity. Therefore, overall skeletal maturity can only be assessed through the identification of widespread EFS presence throughout an individual's skeleton. The presence of an EFS is vital to our interpretations of extinct organisms' life histories. Histological signals of skeletal maturation have been used to assess the validity of distinct non-avian dinosaur taxa (Woodward et al., 2020), assign specimens to specific species (e.g. Cullen et al., 2020), elucidate intraskeletal variation in somatic maturation (e.g. Woodward et al., 2015) and investigate faunal responses to climatic events such as the cataclysmic Permian–Triassic mass extinctions (e.g. Botha-Brink et al., 2016). Here, an EFS is found in the cortices of all hindlimb bones sampled from the male kiwi, but the forelimb cortices are completely remodelled. Likewise, an EFS is present in the tarsometatarsus, tibiotarsus and femora of the female kiwi, but is not present in the forelimbs. In all elements with an EFS, the primary cortical tissue transitions into the outer avascular lamellar/parallel-fibered tissue complex indicative of skeletal maturity. Primary tissue in the female kiwi forelimb elements is PFB with minimal vascularity and little remodelling, characteristics that obscure a transition from typical primary bone growth to skeletal maturity due to their similarity in tissue organization with an EFS. The forelimb elements of the kiwi are extremely small in relation

to the kiwi forelimbs due to flightlessness and appositional bone deposition in smaller long bone elements is, in general, slower compared to deposition rates in larger weight-bearing elements. Lower apposition rates in small long bones result in tissue organization and vascular densities similar to those found in the EFS of larger long bones, thus, obscuring the presence of an EFS in smaller long bones.

The interpretations of osteohistological characters in extinct taxa are dependent on observations made of modern species. Further sampling and investigations of modern taxa are necessary to refine our understanding of the evolution of life histories across vertebrates (e.g. Houssaye, 2014; Wood & de Pietri, 2015). Modern aves present a unique group whose life history characteristics are applicable in interpreting growth and biology of non-avian dinosaurs in addition to fossil neornithines. The findings of this current study impact the interpretations of cortical growth marks, EFS and intraskeletal variation in extinct taxa, but a larger sample of individuals across ontogeny is necessary to confirm and expand upon our results.

6 | CONCLUSIONS

Intraskeletal variation in tissue organization, vascularity and growth mark counts in the North Island brown kiwi has been fully described for the first time. The tarsometatarsus, tibiotarsus, femur, humerus, ulna and radius of a captive raised female kiwi and male kiwi of known age were histologically sampled. Generally, tissue organization reflected the kiwi's low metabolic rates and protracted growth; cortices of hindlimb elements were composed primarily of cyclical parallel-fibered tissue, longitudinal vascular canals, sparse secondary osteons and local regions of CCCB. The 14-year-old male kiwi forelimb cortices exhibited extensive remodelling, obliterating primary tissue and growth marks. Intraskeletal LAG counts in the male kiwi hindlimbs and female kiwi forelimbs and hindlimbs were inconsistent and rarely aligned with known age of each individual. In particular, LAG counts in the female tibiotarsi exceeded the actual age of the individual. We advise caution when using LAGs as age indicators in skeletally mature kiwis, although decoupling of age and LAG deposition may be due, in part, to abnormal resource availability in captivity. This study adds to an increasing extant osteohistological database and serves as a useful comparative tool for the interpretation of growth marks in non-avian dinosaurs.

7 | DATA AVAILABILITY STATEMENT

Figures and additional images available at morphobank.org (P4029).

ACKNOWLEDGEMENTS

The authors would like to thank Todd L. Green for vital discussions concerning palaeognath biology. Paul M. Gignac for discussions and information pertaining to diceCT scanning. Stephen Rigsby at DENTSPLY R&D for initial CT bone scans. Funding for CT scanning was provided by NSF DEB 1457180 to Paul M. Gignac. The authors would also like to thank Alida M. Bailleul, Phil Cox and an anonymous reviewer for critiques that greatly improved the manuscript.

AUTHOR CONTRIBUTIONS

CTH processed specimens, acquired and analysed data, and drafted manuscript. HNW acquired specimens, and provided essential critical revisions of the manuscript.

ORCID

Christian T. Heck https://orcid.org/0000-0003-3252-1698

REFERENCES

Amprino, R. (1947) La structure du tissu osseux envisagée comme expression de différences dans la vitesse de l'accroissement. *Archives de Biologie*, 58, 315–330.

Avrahami, H.M., Makovicky, P. & Zanno, L.E. (2019) Paleohistology of a new orodromine from the Upper Cretaceous (Cenomanian) Mussentuchit Member of the Cedar Mountain Formation, Utah: histological implications for burrowing behavior. *Journal of Vertebrate Paleontology, Programs and Abstracts*, 2019, 56.

Bailleul, A.M., O'Connor, J. & Schweitzer, M.H. (2019) Dinosaur paleohistology: review, trends and new avenues of investigation. *PeerJ*, 7, e7764.

Beale, G. (1985) A radiological study of the kiwi (*Apteryx australis mantelli*). *Journal of the Royal Society of New Zealand*, 15, 187–200.

Beale, G. (1991) The maturation of the skeleton of a kiwi (*Apteryx australis mantelli*) – a ten year radiological study. *Journal of the Royal Society of New Zealand*, 21, 219–220.

Botha-Brink, J., Codron, D., Huttenlocker, A.K., Angielczyk, K.D. & Ruta, M. (2016) Breeding young as a survival strategy during earth's greatest mass extinction. *Scientific Reports*, 6, 24053.

Bourdon, E., Castanet, J., Ricqlès, A.D., Scofield, P., Tennyson, A. & Lamrous, H. et al. (2009) Bone growth marks reveal protracted growth in New Zealand kiwi (Aves, Apterygidae). *Biology Letters*, 5, 639–642.

Broughton, J.M., Rampton, D. & Holanda, K. (2002) A test of an osteologically based age determination technique in the Double-crested Cormorant *Phalacrocorax auritus*. *Ibis*, 144, 143–146.

Bruce, R.C. & Castanet, J. (2006) Application of skeletochronology in aging larvae of the salamanders *Gyrinophilus porphyriticus* and *Pseudotriton ruber*. *Journal of Herpetology*, 40, 85–90.

Burbridge, M., Colbourne, R., Roberson, H. & Baker, A. (2003) Molecular and other biological evidence supports the recognition of at least three species of brown kiwi. *Conservation Genetics*, 4(2), 167–177.

Calder, W.A. & Dawson, T.J. (1978) Resting metabolic rates of ratite birds: the kiwis and the emu. *Comparative Biochemistry and Physiology – Part A: Physiology*, 60(4), 479–481.

Calderon, T., DeMiguel, D., Arnold, W., Stalder, G. & Köhler, M. (2019) Calibration of life history traits with epiphyseal closure, dental eruption and bone histology in captive and wild red deer. *Journal of Anatomy*, 235, 205–216.

Campione, N.E. & Evans, D.C. (2012) A universal scaling relationship between body mass and proximal limb bone dimensions in quadrupedal terrestrial tetrapods. *BMC Biology*, 10, 60.

Canoville, A., Schweitzer, M.H. & Zanno, L.E. (2019) Systemic distribution of medullary bone in the avian skeleton: ground truthing criteria for the identification of reproductive tissues in extinct Avemetatarsalia. *BMC Evolutionary Biology*, 19, 71.

Canoville, A., Schweitzer, M.H. & Zanno, L.E. (2019) Identifying medullary bone in extinct avemetatarsalians: challenges, implications and perspectives. *Philosophical Transactions of the Royal Society B*, 375, 20190133.

Castanet, J., Croci, S., Aujard, F., Perret, M., Cubo, J. & de Margerie, E. (2004) Lines of arrested growth in bone and age estimation in a small primate: *Microcebus murinus*. *Journal of Zoology*, 263, 31–39.

Castanet, J., Francillon-Vieillot, H., Meunier, P. & de Ricqlès, A. (1993) Bone and individual aging. In: Hall, B.K. (Ed.) *Bone*. London: CRC Press, pp. 245–283.

Castanet, J., Rogers, K.C., Cubo, J. & Jacques-Boisard, J. (2000). Periosteal bone growth rates in extant ratites (ostriche and emu). Implications for assessing growth in dinosaurs. *Comptes Rendus de l'Academie des Sciences - Series III - Sciences de la Vie*, 323, 543–550.

Cerda, I.A., Tambussi, C.P. & Degrange, F.J. (2015) Unexpected microanatomical variation among Eocene Antarctic stem penguins (Aves: Sphenisciformes). *Historical Biology*, 27(5), 549–557.

Chinsamy, A., Chiappe, L.M. & Dodson, P. (1995) Mesozoic avian bone microstructure: physiological implications. *Paleobiology*, 21(4), 561–574.

Chinsamy, A., Martin, L.D. & Dodson, P. (1998) Bone microstructure of the diving *Hesperornis* and the voltant *Ichthyornis* from the Niobrara Chalk of western Kansas. *Cretaceous Research*, 19, 225–233.

Cullen, T.M., Evans, D.C., Ryan, M.J., Currie, P.J. & Kobayashi, Y. (2014) Osteohistological variation in growth marks and osteocyte lacunar density in a theropod dinosaur (Coelurosauria: Ornithomimidae). *BMC Evolutionary Biology*, 14, 231.

Cullen, T.M., Simon, D.J., Benner, E.K.C. & Evans, D.C. (2020) Morphology and osteohistology of a large-bodied caenagnathid (Theropoda, Oviraptorosauria) from the Hell Creek Formation (Montana): implications for size-based classifications and growth reconstruction in theropods. *Papers in Paleontology*, 2020, 1–17.

de Ricqlès, A., Bourdon, E., Legendre, L. & Cubo, J. (2016) Preliminary assessment of bone histology in the extinct elephant bird *Aepyornis* (Aves, Palaeognathae) from Madagascar. *Comptes Rendus Palevol*, 15, 197–208.

Early, C.M., Morhardt, A.C., Cleland, T.P., Milensky, C.M., Kavich, G.M. & James, H.F. (2020) Chemical effects of diceCT staining protocols on fluid-preserved avian specimens. *PLOS One*, e0238783.

Enlow, D.H. (1963) *Principles of bone remodeling: an account of post-natal growth and remodeling processes in the long bones and the mandible*. Springfield: Charles C. Thomas.

Erickson, G.M., Rogers, K.C. & Yerby, S.A. (2001) Dinosaurian growth patterns and rapid avian growth rates. *Nature*, 412, 429–432.

Erickson, G.M. & Tumanova, T.A. (2000) Growth curve of *Psittacosaurus mongoliensis* Osborn (Ceratopsia: Psittacosauridae) inferred from long bone histology. *Zoological Journal of the Linnean Society*, 130, 551–566.

Faure-Brac, M.G., Pelissier, F. & Cubo, J. (2019) The influence of plane of section on the identification of bone tissue types in amniotes with implications for paleophysiological inferences. *Journal of Morphology*, 280, 1282–1291.

Francillon-Vieillot, H., de Buffrénil, V., Castanet, J., Geraudie, J., Meunier, F.J. & Sire, J.Y. et al. (1990) Microstructure and mineralization of vertebrate skeletal tissues. In: Carter, J. (Ed.) *Skeletal biomineralization patterns, processes and evolutionary trends*. New York: Van Nostrand Reinhold, pp. 471–548.

García-Martínez, R., Marín-Moratella, N., Jordana, X. & Köhler, M. (2011) The ontogeny of bone growth in two species of dormice: reconstructing life history traits. *Comptes Rendus Palevol*, 10, 489–498.

Garrone, M.C., Cerda, I.A. & Tomassini, R.L. (2021) Ontogenetic variability in the limb bones histology of plains vizcacha (*Lagostomus maximus*, Chinchillidae, Rodentia): implications for life history reconstruction of fossil representatives. *Historical Biology*, 33(4), 558–573. https://doi.org/10.1080/08912963.2019.1648450

Haines, R.W. (1942) The evolution of epiphyses and of enchondral bone. *Biological Reviews of the Cambridge Philosophical Society*, 174, 267–292.

Heck, C.T., Varricchio, D.J., Gaudin, T.J., Woodward, H.N. & Horner, J.R. (2019) Ontogenetic changes in the long bone microstructure in the nine-banded armadillo (*Dasypus novemcinctus*). *PLoS One*, 14(4), e0215655.

Holdaway, R.N., Worthy, T.H. & Tennyson, A. (2001) A working list of breeding bird species of the New Zealand region at first human contact. *New Zealand Journal of Zoology*, 28, 119–187.

Horner, J.R., Ricqlès, A.D., & Padian, K. (1999) Variation in dinosaur skeletochronology indicators: implications for age assessment and physiology. *Paleobiology*, 25, 295–304.

Horner, J.R., Woodward, H.N. & Bailleul, A.M. (2016) Mineralized tissues in dinosaurs interpreted as having formed through metaplasia: a preliminary evaluation. *Comptes Rendus Palevol*, 15, 176–196.

Houssaye, A. (2014) Advances in vertebrate palaeohistology: recent progress, discoveries, and new approaches. *Biological Journal of the Linnean Society*, 112, 645–648.

Hübner, T.R. (2012) Bone histology in *Dysalotosaurus lettowvorbecki* (Ornithischia: Iguanodontia) – variation, growth, and implications. *PLoS One*, 7, e22958.

Hugi, J. & Sánchez-Villagra, M.R. (2012) Life history and skeletal adaptations in the galapagos marine iguana (*Amblyrhynchus cristatus*) as reconstructed with bone histological data – a comparative study of iguanines. *Journal of Herpetology*, 46, 312–324.

Huttenlocker, A.K., Woodward, H.N. & Hall, B.K. (2013) The biology of bone. In: Padian, K. & Lamm, E.-T. (Eds.) *Bone histology of fossil tetrapods: advancing methods, analysis, and interpretation*. Berkeley, CA: University of California Press, pp. 13–34.

Kastschenko, M. (1881) Über die Genese und Architektur der Batrachier Knochen. *Archiv für Mikroskopische Anatomie*, 19, 1–52.

Kiwi Captive Management Advisory Committee. (2004) *Captive management plan for kiwi: Apteryx rowi, Apteryx australis, Apteryx australis 'Haast', Apteryx haastii, Apteryx owenii*. Threated species occassional publication. Wellington: New Zealand Department of Conservation.

Klein, N. & Sander, M.P. (2007) Bone histology and growth of the prosauropod dinosaur *Plateosaurus engelhardti* von Meyer, 1837 from the Norian bonebeds of Trossingen (Germany) and Frick (Switzerland). *Special Papers in Palaeontology*, 77, 169–206.

Klein, N., Verrière, A., Sartorelli, H., Wintrich, T. & Fröbisch, J. (2019) Microanatomy and growth of the mesosaurs *Stereosternum tumidum* and *Brazilosaurus sanpauloensis* (Reptilia, Parareptilia). *Fossil Record*, 22, 91–110.

Klevezal, G.A. (1996) *Recording structures of mammals: determination of age and reconstruction of life history*. Brookfield: A.A. Balkema Publishers.

Klomp, N.I. & Furness, R.W. (1992) A technique which may allow accurate determination of the age of adult birds. *Ibis*, 134, 245–249.

Köhler, M., Marín-Moratalla, N., Jordana, X. & Aanes, R. (2012) Seasonal bone growth and physiology in endotherms shed light on dinosaur physiology. *Nature*, 487, 358–361.

Kolb, C., Scheyer, T.M., Veitschegger, K., Forasiepi, A.M., Amson, E. & Van der Geer, A.E. et al. (2015) Mammalian bone palaeohistology: a survey and new data with emphasis on island forms. *PeerJ*, 3, e1358.

Kuehn, A.L., Lee, A.H., Main, R.P. & Simons, E.L.R. (2019) The effects of growth rate and biomechanical loading on bone laminarity within the emu skeleton. *PeerJ*, 7, e7616.

Lee, A.H. & O'Connor, P.M. (2013) Bone histology confirms determinate growth and small body size in the noasaurid theropod *Masiakosaurus knopfleri*. *Journal of Vertebrate Paleontology*, 33, 865–876.

Lee, A.H. & Werning, S. (2008) Sexual maturity in growing dinosaurs does not fit reptilian growth models. *Proceedings of the National Academy of Sciences of the USA*, 105(2), 582–587.

Lee, D.E., Lee, W.G. & Mortimer, N. (2001) Where and why have all the flowers gone? Depletion and turnover in the New Zealand Cenozoic angiosperm flora in relation to palaeogeography and climate. *Australian Journal of Botany*, 49, 341–356.

Legendre, L.J. & Botha-Brink, J. (2018) Digging the compromise: investigating the link between limb bone histology and fossoriality in the aardvark (*Orycteropus afer*). *PeerJ*, 6, e5216.

Legendre, L., Bourdon, E., Scofield, R.P., Tennyson, A.J.D., Lamrous, H. & de Ricqles, A. et al. (2014) Bone histology, phylogeny, and palaeognathous birds (Aves: Palaeognathae). *Biological Journal of the Linnean Society*, 112, 688–700.

Mallon, J.C. (2017) Recognizing sexual dimorphism in the fossil record: lessons from nonavian dinosaurs. *Paleobiology*, 43(3), 495–507.

Marín-Moratalla, N., Jordana, X. & Köhler, M. (2013) Bone histology as an approach to providing data on certain key life history traits in mammals: implications for conservation biology. *Mammalian Biology*, 78, 422–429.

Marsà, J.A.G., Agnolin, F.L. & Novas, F. (2019) Bone microstructure of *Vegavis iaai* (Aves, Anseriformes) from the Upper Cretaceous of Vega Island, Antarctic Peninsula. *Historical Biology*, 31(2), 163–167.

McGowan, C. (1979) The hind limb musculature of the brown kiwi, *Apteryx australis mantelli*. *Journal of Morphology*, 160, 33–74.

McLennan, J.A., Dew, L., Miles, J., Gillingham, N. & Waiwai, R. (2004) Size matters: predation risk and juvenile growth in North Island brown kiwi (*Apteryx mantelli*). *New Zealand Journal of Ecology*, 28(2), 241–250.

McLennan, J.A., Potter, M.A., Robertson, H.A., Wake, G.C., Colbourne, R.M. & Dew, L. et al. (1996) Role of predation in the decline of kiwi, *Apteryx* spp., in New Zealand. *New Zealand Journal of Ecology*, 20, 27–35.

McNab, B.K. (1994) Energy conservation and the evolution of flightlessness in birds. *American Naturalist*, 144(4), 628–642.

Montoya-Sanhueza, G. & Chinsamy, A. (2017) Long bone histology of the subterranean rodent *Bathyergus suillus* (Bathyergidae): ontogenetic pattern of cortical bone thickening. *Journal of Anatomy*, 230, 203–233.

Morris, P.A. (1970) A method for determining absolute age in the hedgehog. *Journal of Zoology*, 161, 277–280.

Nacarino-Meneses, C., Jordana, X. & Köhler, M. (2016) First approach to bone histology and skeletochronology of *Equus hemionus*. *Comptes Rendus Palevol*, 15, 267–277.

Nacarino-Meneses, C. & Köhler, M. (2018) Limb bone histology records birth in mammals. *PLoS One*, 13(6), e0198511.

O'Donnel, C.F.J., Weston, K.A. & Monks, J.M. (2017) Impacts of introduced mammalian predators on New Zealand's alpine fauna. *New Zealand Journal of Ecology*, 41(1), 1–22.

Padian, K. (2013) Why study the bone microstructure of fossil tetrapods? In: Padian, K. & Lamm, E.-T. (Eds.) *Bone histology of fossil tetrapods: advancing methods, analysis, and interpretation*. Berkeley, CA: University of California Press.

Padian, K. & Lamm, E.-T. (Eds) (2013) *Bone histology of fossil tetrapods: advancing methods, analysis, and interpretation*. Berkeley, CA: University of California Press.

Padian, K., Lamm, E.-T. & Werning, S. (2013) Selection of specimens. In: Padian, K. & Lamm, E.-T. (Eds.) *Bone histology of fossil tetrapods: advancing methods, analysis, and interpretation*. Berkeley, CA: University of California Press.

Padian, K., Werning, S. & Horner, J.R. (2016) A hypothesis of differential secondary bone formation in dinosaurs. *Comptes Rendus Palevol*, 15, 40–48.

Ponton, F., Elzanowski, A., Castanet, J., Chinsamy, A., de Margerie, E. & de Ricqles, A. et al. (2004) Variation of the outer circumferential layer in the limb bones of birds. *Acta Ornithologica*, 39, 137–140.

Potter, M.A., Fordham, R.A. & McLennan, J.A. (1996). Reproductive biology of the kiwi. In Deeming, D.C. (Ed.), *Improving our understanding of ratites in a farming environment* (pp. 161–162). Oxfordshire, UK: Ratite Conference.

Prier, E.A., Gartrell, B.D., Potter, M.A., Lopez-Villalobos, N. & McLennan, J. (2013) Characterization of hatch-size and growth rates of captive and wild-reared brown kiwi (*Apteryx mantelli*) chicks. *Zoo Biology*, 32, 541–548.

Prinzinger, R. & Dietz, V. (2002) Pre- and postnatal energetics of the North Island brown kiwi (*Apteryx mantelli*). *Comparative Biochemistry and Physiology Part A: Molecular and Integrative Physiology*, 131(4), 725–732.

Prondvai, E., Stein, K.H.W., de Ricqlès, A. & Cubo, J. (2014) Development-based revision of bone tissue classification: the importance of semantics for science. *Biological Journal of the Linnean Society*, 112, 799–816.

Robertson, H.A., Colbourne, R.M., Graham, P.J., Miller, P.J. & Pierce, R.J. (2011) Experimental management of Brown Kiwi *Apteryx mantelli* in central Northland, New Zealand. *Bird Conservation International*, 21, 207–220.

Rogers, K.C., Whitney, M.R., D'Emic, M. & Bagley, B. (2016) Precocity in a tiny titanosaur from the Cretaceous of Madagascar. *Science*, 352(6284), 450–453.

Sales, J. (2005) The endangered kiwi: a review. *Folia Zoologica*, 54, 1–20.

Sander, P.M. & Andrassy, P. (2006) Lines of arrested growth and long bone histology in Pleistocene large mammals from Germany: what do they tell us about dinosaur physiology? *Palaeontographica Abt A*, 277, 143–159.

Schweitzer, M.H., Elsey, R.M., Dacke, C.G., Horner, J.R. & Lamm, E.-T. (2007) Do egg-laying crocodilian (*Alligator mississippiensis*) archosaurs form medullary bone? *Bone*, 40, 1152–1158.

Schweitzer, M.H., Wittmeyer, J. & Horner, J.R. (2005) Gender-specific reproductive tissue in ratites and *Tyrannosaurus rex*. *Science*, 308(5727), 1456–1460.

Schweitzer, M.H., Zheng, W., Zanno, L., Werning, S. & Sugiyama, T. (2016) Chemistry supports the identification of gender-specific reproductive tissue in *Tyrannosaurus rex*. *Scientific Reports*, 6, 23099.

Skedros, J.G., Sybrowsky, C.L., Parry, T.R. & Bloebaum, R.D. (2003) Regional differences in cortical bone organization and microdamage prevalence in Rocky Mountain mule deer. *Anatomical Record Part A*, 274A, 837–850.

Smith, N.A. & Clarke, J.A. (2014) Osteological histology of the Pan-Alcidae (Aves, Charadriiformes): correlates of wing-propelled diving and flightlessness. *Anatomical Record* 297, 188–199.

Starck, J.M. & Chinsamy, A. (2002) Bone microstructure and developmental plasticity in birds and other dinosaurs. *Journal of Morphology*, 254, 232–246.

Stein, K. & Prondvai, E. (2014) Rethinking the nature of fibrolamellar bone: an integrative biological revision of sauropod plexiform bone formation. *Biological Reviews*, 89, 24–47.

Stein, K. & Sander, M.P. (2009). Histological core drilling: a less destructive method for studying bone histology. In Brown, M., Kane, J. & Parker, W. (Eds.), *Methods in fossil preparation: proceedings of the first annual fossil preparation and collections symposium* (pp. 69–80).

Turvey, S.T., Green, O.R. & Holdaway, R.N. (2005) Cortical growth marks reveal extended juvenile development in New Zealand moa. *Nature Letters*, 435, 940–943.

Walker, M.M., Louys, J., Herries, A.I.R., Price, G.J. & Miszkiewicz, J.J. (2020) Humerus midshaft histology in a modern and fossil wombat. *Australian Mammalogy*, 43(1), 30–39.

Weir, J.T., Haddrath, O., Robertson, H.A., Colbourne, R.M. & Baker, A.J. (2016) Explosive ice age diversification of kiwi. *Proceedings of the National Academy of Sciences of the USA*, 113(38), E5580–E5587.

Werning, S. (2012) The ontogenetic osteohistology of *Tenontosaurus tilletti*. *PLoS One*, 7(3), e33539.

Werning, S. (2018) Medullary bone is phylogenetically widespread and its skeletal distribution varies by taxon. *Journal of Ornithology*, 159, 527–543.

Wilson, L.E. & Chin, K. (2014) Comparative osteohistology of *Hesperornis* with reference to pygoscelid penguins: the effects of climate and behavior on avian bone microstructure. *Royal Society Open Science*, 1, 140245.

Wood, J.R. & de Pietri, V.L. (2015) Next-generation paleornithology: technological and methodological advances allow new insights into the evolutionary and ecological histories of living birds. *The Auk*, 132, 486–506.

Woodward, H.N., Freedman Fowler, E.A., Farlow, J.O. & Horner, J.R. (2015) *Maiasaura*, a model organism for extinct vertebrate population biology: a large sample statistical assessment of growth dynamics and survivorship. *Paleobiology*, 41(4), 503–527.

Woodward, H.N., Horner, J.R. & Farlow, J.O. (2014) Quantification of intraskeletal histovariability in *Alligator mississippiensis* and implications for vertebrate osteohistology. *PeerJ*, 2, e422.

Woodward, H.N., Padian, K. & Lee, A.H. (2013) Skeletochronology. In: Padian, K. & Lamm, E.-T. (Eds.) *Bone histology of fossil tetrapods: advancing methods, analysis, and interpretation*. Berkeley, CA: University of California Press, pp. 195–215.

Woodward, H.N., Rich, T.H. & Vickers-Rich, P. (2018) The bone microstructure of polar "hypsilophodontid" dinosaurs from Victoria, Australia. *Scientific Reports*, 2018(8), 1162.

Woodward, H.N., Tremaine, K., Williams, S.A., Zanno, L.E., Horner, J.R. & Myhrvold, N. (2020) Growing up *Tyrannosaurus rex*: osteohistology refutes the pygmy "Nanotyrannus" and supports ontogenetic niche partitioning in juvenile *Tyrannosaurus*. Science. *Advances*, 6(1), eaax6250.

SUPPORTING INFORMATION

Additional supporting information may be found online in the Supporting Information section.

How to cite this article: Heck, C.T.&Woodward, H.N. (2021) Intraskeletal bone growth patterns in the North Island Brown Kiwi (*Apteryx mantelli*): Growth mark discrepancy and implications for extinct taxa. *Journal of Anatomy*, 239, 1075–1095. https://doi.org/10.1111/joa.13503